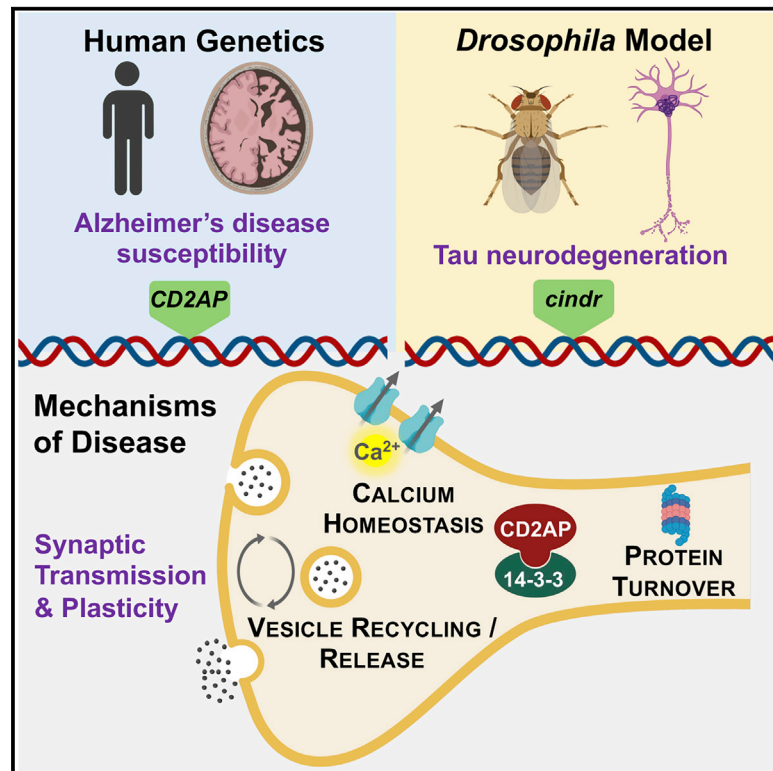


cindr, the *Drosophila* Homolog of the **CD2AP** Alzheimer's Disease Risk Gene, Is Required for Synaptic Transmission and Proteostasis

Graphical Abstract



Authors

Shamsideen A. Ojelade, Tom V. Lee, Nikolaos Giagtzoglou, ..., Benjamin R. Arenkiel, Hugo J. Bellen, Joshua M. Shulman

Correspondence

joshua.shulman@bcm.edu

In Brief

CD2AP is an Alzheimer's disease susceptibility gene with uncertain brain function. Ojelade et al. discover that mutation of the *Drosophila* homolog *cindr* disrupts ubiquitin-proteasome system activity, causing calcium dyshomeostasis and impaired synaptic vesicle recycling and release. *Cd2ap* null mice and human brain proteomic studies support a conserved role in synaptic proteostasis.

Highlights

- *cindr*, fly homolog of the Alzheimer's risk gene *CD2AP*, encodes a synaptic protein
- *cindr* mutants disrupt synaptic vesicle recycling and release and impair plasticity
- *Cindr* and 14-3-3 ζ regulate the proteasome and presynaptic calcium homeostasis
- *Cd2ap* mouse and human brain studies support a conserved role in synapse proteostasis



cindr, the *Drosophila* Homolog of the *CD2AP* Alzheimer's Disease Risk Gene, Is Required for Synaptic Transmission and Proteostasis

Shamsideen A. Ojelade,^{1,2} Tom V. Lee,^{1,2} Nikolaos Giagtzoglou,^{1,2,11} Lei Yu,³ Berrak Ugur,^{4,12} Yarong Li,^{1,2} Lita Duraine,⁵ Zhongyuan Zuo,⁵ Vlad Petyuk,⁶ Philip L. De Jager,^{7,8} David A. Bennett,³ Benjamin R. Arenkiel,^{2,4,5,9} Hugo J. Bellen,^{2,4,5,9,10} and Joshua M. Shulman^{1,2,4,5,9,13,*}

¹Department of Neurology, Baylor College of Medicine, Houston, TX 77030, USA

²Jan and Dan Duncan Neurologic Research Institute, Texas Children's Hospital, Houston, TX 77030, USA

³Rush Alzheimer's Disease Center, Rush University Medical Center, Chicago, IL 60612, USA

⁴Program in Developmental Biology, Baylor College of Medicine, Houston, TX 77030, USA

⁵Department of Molecular & Human Genetics, Baylor College of Medicine, Houston, TX 77030, USA

⁶Pacific Northwest National Laboratory, Richland, WA 99354, USA

⁷Center for Translational & Computational Neuroimmunology, Department of Neurology and the Taub Institute, Columbia University Medical Center, New York, NY 10032, USA

⁸Cell Circuits Program, Broad Institute, Cambridge, MA 02142, USA

⁹Department of Neuroscience, Baylor College of Medicine, Houston, TX 77030, USA

¹⁰Howard Hughes Medical Institute, Baylor College of Medicine, Houston, TX 77030, USA

¹¹Present address: Amgen, Neuroscience, Cambridge, MA 02142, USA

¹²Present address: Howard Hughes Medical Institute and Department of Neuroscience, Yale University School of Medicine, New Haven, CT 06520, USA

¹³Lead Contact

*Correspondence: joshua.shulman@bcm.edu

<https://doi.org/10.1016/j.celrep.2019.07.041>

SUMMARY

The Alzheimer's disease (AD) susceptibility gene, CD2-associated protein (*CD2AP*), encodes an actin binding adaptor protein, but its function in the nervous system is largely unknown. Loss of the *Drosophila* ortholog *cindr* enhances neurotoxicity of human Tau, which forms neurofibrillary tangle pathology in AD. We show that *Cindr* is expressed in neurons and present at synaptic terminals. *cindr* mutants show impairments in synapse maturation and both synaptic vesicle recycling and release. *Cindr* associates and genetically interacts with 14-3-3 ζ , regulates the ubiquitin-proteasome system, and affects turnover of Synapsin and the plasma membrane calcium ATPase (PMCA). Loss of *cindr* elevates PMCA levels and reduces cytosolic calcium. Studies of *Cd2ap* null mice support a conserved role in synaptic proteostasis, and CD2AP protein levels are inversely related to Synapsin abundance in human postmortem brains. Our results reveal CD2AP neuronal requirements with relevance to AD susceptibility, including for proteostasis, calcium handling, and synaptic structure and function.

INTRODUCTION

Alzheimer's disease (AD) is a progressive and incurable neurodegenerative disorder that is estimated to affect 13 million

people in the United States by 2050 (Alzheimer's Association, 2016). At autopsy, AD is characterized by extracellular neuritic plaques and intraneuronal neurofibrillary tangles, predominantly composed of misfolded and aggregated β -amyloid ($A\beta$) peptide and the microtubule-associated protein tau (MAPT or Tau), respectively (Scheltens et al., 2016). Substantial evidence indicates that AD pathology disrupts synaptic function at an early stage, and synapse loss is strongly associated with clinical progression (Spires-Jones and Hyman, 2014). Human genome-wide association studies (GWASs) have discovered nearly 30 common variants associated with AD risk (Jansen et al., 2019; Kunkle et al., 2019; Lambert et al., 2013); however, most of these newly implicated genes remain poorly studied, especially in the nervous system. In prior work, we leveraged a human MAPT transgenic model in the fruit fly, *Drosophila melanogaster*, to identify AD susceptibility gene candidates that interact with Tau-mediated mechanisms (Shulman et al., 2014). Among our findings, knockdown of *cindr*, the ortholog of the AD risk gene CD2-associated protein (*CD2AP*), enhanced Tau-induced neurodegeneration.

Before its identification from AD GWASs, loss-of-function mutations in *CD2AP* were identified as a rare cause of familial, autosomal dominant, focal segmental glomerulosclerosis, and progressive renal dysfunction has been recapitulated in mice hetero- or homozygous for a *Cd2ap* knockout allele (Kim et al., 2003; Shih et al., 1999). *CD2AP* encodes an adaptor protein that contains three SH3 motifs, a proline-rich region, and an actin binding domain (Dustin et al., 1998). In the kidney, *CD2AP* is required to maintain structural integrity of the slit diaphragm, the specialized junctions between the foot processes of glomerular podocytes. Additional studies support a role for CD2AP in



cytoskeletal anchoring of adhesion complexes (Johnson et al., 2008; Lynch et al., 2003) and regulation of membrane localization for cell surface receptors via endocytosis (Johnson et al., 2012; Minegishi et al., 2013). Several other AD susceptibility loci harbor genes with links to cell adhesion (*CASS4*, *FERMT2*, and *PTK2B*) and endocytosis (*BIN1*, *PICALM*, and *RIN3*). Nevertheless, the function of *CD2AP* in the adult nervous system, or its mechanism in neurological disorders, remains largely unknown. Studies in mice have connected *CD2AP* to both axonal growth (Harrison et al., 2016) and maintenance of blood-brain barrier integrity (Cochran et al., 2015). *CD2AP* has also been implicated in amyloid precursor protein trafficking and processing in cultured neurons (Ubelmann et al., 2017), although *Cd2ap* loss of function did not affect total A β levels or amyloid plaque burden in AD mouse models (Liao et al., 2015).

Besides suggesting potential interactions with Tau (Shulman et al., 2014), investigations in the fruit fly have implicated *cindr* with conserved roles in nephrocytes (Fu et al., 2017), retinal development (Johnson et al., 2008, 2012), and oogenesis (Haglund et al., 2010). Here, we have used *Drosophila* to elucidate the role of *cindr* in the nervous system, confirming a requirement for synaptic vesicle endocytosis and revealing requirements for ubiquitin-proteasome-mediated protein turnover and presynaptic Ca²⁺ homeostasis. Moreover, we present evidence that the role of *CD2AP* in synaptic proteostasis is conserved in the mammalian brain and may contribute to vulnerability for Tau-mediated neurotoxic mechanisms in AD.

RESULTS

Cindr Is Expressed in the Nervous System and Associates with Synaptic Proteins

We first characterized the expression and subcellular localization of Cindr in the *Drosophila* nervous system (Figures 1 and S1). Consistent results were obtained using either a published anti-Cindr antibody (Johnson et al., 2008) or an available allele, *cindr*^{CA06686} (Buszczak et al., 2007), referred to hereafter as *cindr*^{GFP}, that encodes a functional, GFP-tagged protein under the control of endogenous genomic regulatory elements (Figure 1A). Neither Cindr^{GFP} nor anti-Cindr antibody permit detection of all predicted, alternative protein isoforms. Nevertheless, *cindr* appears to be expressed ubiquitously, including in both the adult and the larval nervous system (Figures 1 and S1). In the adult brain, Cindr appears enriched within the neuropil, where it colocalizes with the presynaptic marker Bruchpilot (nc82) (Wagh et al., 2006) (Figure 1B). Cindr is also present at photoreceptor presynaptic terminals in the lamina (Figure S1C). Besides widespread neuronal expression, Cindr is detectable in glial cells (Figure S1E). In larval preparations, Cindr staining reveals a punctate distribution within the body wall musculature and appears enriched predominantly at the presynapse of the neuromuscular junction (NMJ) (Figures 1C and S1F). Within the presynaptic bouton, Cindr is detectable both at the membrane and in a predominantly patchy, cytoplasmic distribution in which puncta are also observed (Figures 1D and S1F).

To identify proteins that interact with Cindr, we performed immunoprecipitation (IP) followed by mass spectrometry (MS). Homogenates from adult fly heads were prepared from *cindr*^{GFP}

animals, and IP was performed using a high-affinity anti-GFP antibody (Neumüller et al., 2012). Based on MS peptide counts, Cindr associates with actin, as expected, and several other candidate binding partners, including proteins related to synaptic transmission (Table S1). Directed coimmunoprecipitation (coIP) was performed for independent confirmation of selected interaction partners (Figure 1E). For these experiments, we expressed Cindr using the pan-neuronal driver *Elav-GAL4* and a cDNA transgene encoding a Cindr:GFP fusion protein under control of the heterologous upstream activating sequence (*UAS*) (*Elav>cindr*). We confirmed the interaction with actin and validated associations with presynaptic proteins, including the Ca²⁺ sensor Synaptotagmin (Littleton et al., 1993b) and the synaptic vesicle reserve pool marker Synapsin (Klagges et al., 1996; Cesca et al., 2010). Cindr showed partially overlapping localization *in vivo* with potential synaptic binding partners at the larval NMJ, including both Synapsin and Synaptotagmin (Figure 1D). Cindr also bound the plasma membrane calcium ATPase (PMCA), a regulator of calcium homeostasis; 26S regulatory proteasomal subunit 5 (Rpt5); and the homolog of the adaptor protein 14-3-3 ζ , known as Leonardo in *Drosophila*, which has been previously implicated in synaptic function (Broadie et al., 1997; Skoulakis and Davis, 1996). Based on its localization and interaction partners, these data suggest that Cindr may play a role at the synapse in *Drosophila*.

***cindr* Is Required for Synaptic Maturation**

Prior studies of *cindr* in *Drosophila* have relied on knockdown experiments with RNAi strains or transgenic overexpression (Johnson et al., 2008; Fu et al., 2017). We generated a null allele, *cindr*¹, via Flippase (FLP)-mediated recombination between two flanking PiggyBac transposable elements harboring Flippase recognition target (FRT) sites (Cook et al., 2012; Ryder et al., 2007), deleting the entire gene (Figure 1A). *cindr* mRNA transcripts were undetectable in *cindr*¹ homozygotes, confirming that it is a null allele (Figure S1A). In homozygosity, *cindr*¹ is semi-lethal, with approximately 30% of the expected number of adults eclosing (Figure S2B), and we found similar reduced viability and survival (Figure 2A) when *cindr*¹ was crossed to a deficiency strain (*Df(3R)Exel6217*), which deletes most of the *cindr* locus after the 3rd exon (Figure 1A). In *cindr*¹/*Df(3R)Exel6217* trans-heterozygotes (hereafter called *cindr*^{1/Df}), we documented an 88% reduction in mRNA transcripts (Figure S1A), and Cindr protein was undetectable in the adult brain using anti-Cindr, which is directed against a C-terminal epitope (Figure S1B). Based on our studies, *cindr*^{1/Df} produces phenotypes consistent with that of the confirmed molecular null genotype *cindr*¹, and in all cases loss-of-function phenotypes were fully rescued by either a 38- or a 90-kb P[acman] bacterial artificial chromosome (Venken et al., 2009) containing the *cindr* genomic locus (Figure 1A). We cannot exclude the possibility of expression of a truncated Cindr protein in *cindr*^{1/Df} animals, comprising a 350 amino acid, N-terminal fragment including the SH3 domains only (Figure S2A); however, if present, our data suggest it is unlikely to be functional.

To elucidate potential requirements for *cindr* in CNS development and/or maintenance, we examined aged adults. Based on H&E staining of paraffin brain sections, we did not observe

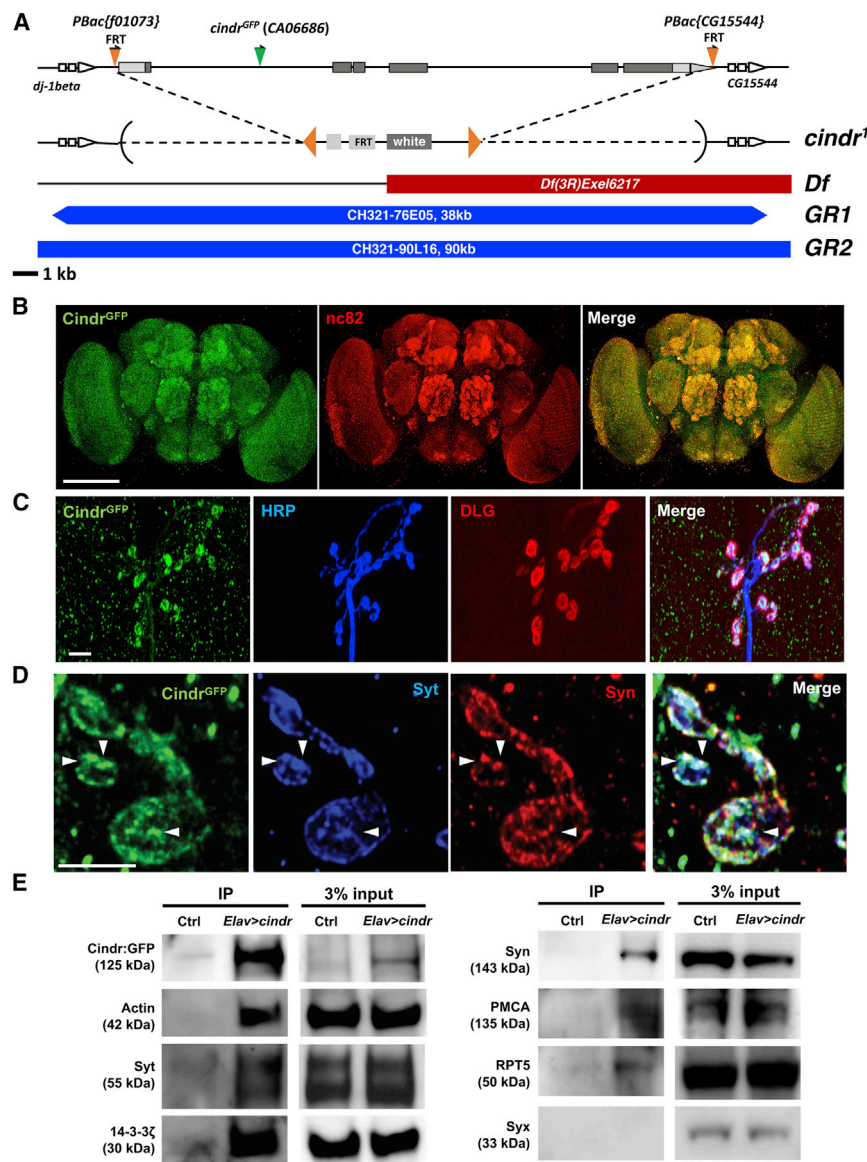


Figure 1. Cindr Is Present at Synapses and Associates with Other Synaptic Proteins

(A) *cindr* genomic locus is shown, including coding exons (dark gray), untranslated regions (light gray), and transposon insertion alleles (triangles) used in this study. *cindr^{CA06686}* (green) contains a GFP coding exon, flanked by splice acceptor and donor sequences and resulting in an N-terminal tagged-Cindr protein (*Cindr^{GFP}*). Recombination was performed between 2 FRT-containing piggyBac insertions (orange) flanking the *cindr* locus. In the null allele *cindr¹*, the gene coding sequence is replaced with a hybrid transposable element containing a *mini-white* gene. A chromosomal deficiency, *Df(3R)Exel6217*, is shown (*Df*, red), along with two bacterial artificial chromosomes (BACs) (blue), used for transgenic genomic rescue constructs (*GR1* and *GR2*). See also Figure S2A for Cindr protein structure.

(B–D) Cindr expression and subcellular localization were assayed using *Cindr^{GFP}*, enhanced by staining with anti-GFP. See also Figure S1.

(B) In the adult brain, *Cindr^{GFP}* (green) is predominantly within the neuropil and colocalizes with the presynaptic active zone marker Bruchpilot (*nc82*) (red). Scale bar, 100 μ m.

(C) In the larval peripheral nervous system, *Cindr^{GFP}* (green) reveals a punctate distribution in the body wall muscles and is enriched within the synaptic terminal boutons at neuromuscular junctions, where it predominantly colocalizes with the presynaptic marker horseradish peroxidase (anti-HRP) (blue), but not the postsynaptic membrane marker discs large (anti-DLG) (red). Scale bar, 10 μ m.

(D) *Cindr^{GFP}* (green) shows partially overlapping localization (arrowheads) with candidate binding partners at the neuromuscular junction, including Synapsin (anti-Syn) (red) and Synaptotagmin (anti-Syt) (blue). Scale bar, 10 μ m.

(E) Candidate Cindr binding partners were confirmed using pull-down assays from head homogenates. Cindr coimmunoprecipitates with actin, Synaptotagmin (Syt), 14-3-3 ζ , Synapsin (Syn), plasma membrane calcium ATPase (PMCA), and regulatory proteasome subunit 5 (Rpt5), but not Syntaxin (Syx).

obvious morphological defects or evidence of neurodegeneration in 30-day-old *cindr^{1/Df}* or *cindr¹* animals (Figures 2B and S2C). However, consistent with previous studies in flies (Johnson et al., 2008) and mammalian cells (Zhao et al., 2013a), rhodamine-phalloidin staining revealed increased F-actin throughout the adult brain of *cindr^{1/Df}* animals (Figure S3A). Prior published work has implicated *cindr* in developmental patterning of the retina (Johnson et al., 2008), but based on transmission electron microscopy (TEM), we did not detect overt evidence of ommatidial patterning defects or retinal degeneration in aged *cindr^{1/Df}* adults (Figures 2B and S4). We also confirmed normal patterning of photoreceptor projections in the lamina (Figures S3C and S4), and electroretinograms did not reveal detectable impairment in phototransduction (Figure S3D). Nevertheless, we cannot exclude a retinal requirement for *cindr* that resolves before eclosion of homozygous adult escapers or during aging,

because prior studies focused on pupal stages (Johnson et al., 2008, 2011, 2012).

Given its enrichment at presynaptic terminals and interaction with synaptic proteins, we next explored a potential requirement for Cindr at synapses, taking advantage of the larval NMJ (Bellen et al., 2010; Frank et al., 2013; Harris and Littleton, 2015). Based on confocal microscopy, neither bouton size nor overall number of synaptic terminals was altered in *cindr^{1/Df}* animals (Figures S5A and S5B). We next stained for several synaptic vesicle-associated proteins, including Synaptotagmin and Synapsin, which both coIP with Cindr. While the expression and distribution of Synaptotagmin and EPS15 appeared normal (Figures S5C–S5F), we discovered a nearly 2-fold increase in Synapsin protein levels in *cindr^{1/Df}* animals (Figures 2C and 2E). In addition, when costaining for pre- and postsynaptic markers, we noted an increase in the number of incompletely differentiated boutons in

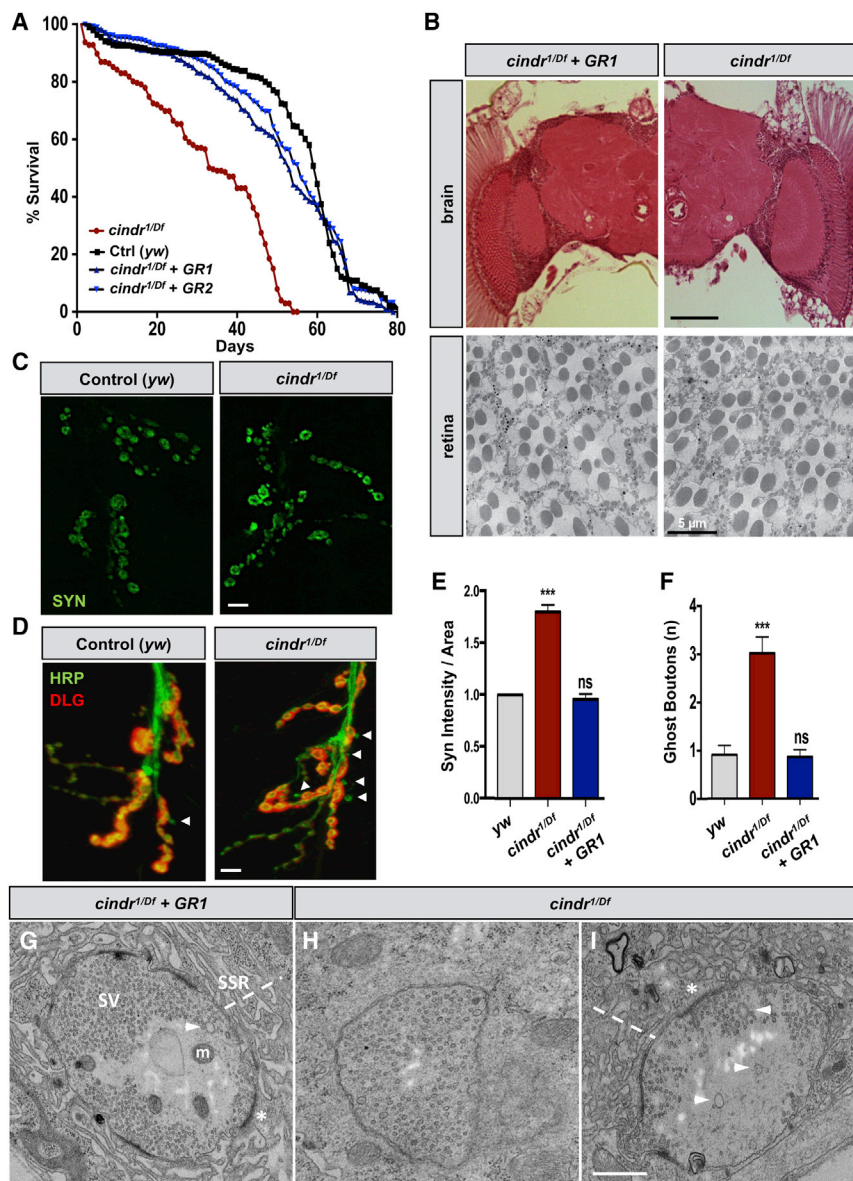


Figure 2. *cindr* Is Dispensable for Development and Maintenance of the Adult Brain but Is Required for Synapse Maturation at the NMJ

(A) *cindr*^{1/Df} flies (*cindr*^{1/Df(3R)Exel6217}) show reduced survival that is rescued by either heterozygous *GR1* or *GR2* transgenic BAC constructs. (B) Top: H&E staining of frontal brain sections from 30-day-old *cindr*^{1/Df} or controls (*cindr*^{1/Df} + *GR1*) demonstrate no overt neuronal loss or other apparent pathology. Scale bar, 50 μ m. See also Figure S2C. Bottom: transmission electron micrographs of tangential retinal sections reveal normal architecture in 30-day-old animals, including photoreceptor clusters and surrounding pigment cells, comprising the ommatidia. Scale bar, 5 μ m. See also Figure S4.

(C) Levels of Synapsin protein (anti-Syn) (green) at the larval neuromuscular junction are increased in *cindr*^{1/Df} animals versus control (*yw*). Scale bar, 10 μ m.

(D) *cindr* loss of function causes an increased number of ghost boutons (arrows). Incompletely differentiated terminals are identified by the presence of the presynaptic marker horseradish peroxidase (anti-HRP) (green) but absence of surrounding postsynaptic membranes, colabeled with discs large (anti-DLG) (red). Scale bar, 10 μ m. See also Figure S3B.

(E and F) Quantification ($n > 10$) of Synapsin immunofluorescence (E) and ghost boutons (F), as shown in (C) and (D), respectively. All error bars denote SEM. *** $p < 0.001$; ns, not significant. See also Figure S5.

(G–I) Electron micrographs of larval neuromuscular junctions. Control synaptic terminals (G) are surrounded by a sub-synaptic reticulum (SSR) associated with the postsynaptic membrane (dotted line). Normal appearance of the active zone (asterisk), synaptic vesicles (SV), and mitochondrion (m) is also indicated. In *cindr* mutants, synaptic defects include (H) synaptic terminals lacking a sub-synaptic reticulum and (I) boutons with decreased synaptic vesicle density. *cindr* mutant synaptic terminals are also characterized by increased numbers of enlarged vesicles (arrowheads in G and I). Scale bar, 600 nm. See also Figure S6.

either *cindr*^{1/Df} or *cindr*¹ animals (Figures 2D, 2F, S2D, and S3B). Such NMJ terminals that show labeling with presynaptic markers, but not postsynaptic markers, have been termed ghost boutons (Packard et al., 2002) and can be observed in mutants that disrupt synaptic differentiation and/or activity-dependent synaptic remodeling (Ataman et al., 2008; Piccioli and Littleton, 2014; Vasin et al., 2014). We validated that the *cindr* genomic construct fully rescues both the ghost bouton phenotype and the Synapsin protein elevations (Figures 2E and 2F). We confirmed rescue of the *cindr*^{1/Df} ghost bouton phenotype by cell-type-specific expression of *cindr* in neurons (*Elav>cindr*) (Figure S5G), consistent with a cell autonomous requirement.

To determine synaptic bouton ultrastructure, we performed TEM in *cindr*^{1/Df} larvae (Figures 2G–2I and S6). A substantial proportion (13%) of *cindr*^{1/Df} NMJ boutons lacked a sub-synaptic re-

ticulum and active zones (Figures 2H and S6E), and they likely correspond to ghost boutons detected by confocal microscopy (Figure 2D). We never observed this phenotype in TEM of controls (*GR1/+; cindr*^{1/Df}). Following *cindr* loss of function, synaptic terminals frequently were abnormally elongated, consistent with impaired differentiation and/or maintenance of synaptic morphology (Figures S6B and S6E). Overall, *cindr*^{1/Df} NMJ boutons exhibited a 43% reduction in mean synaptic vesicle density, along with increased numbers of aberrant, enlarged vesicles (Figures 2I, S6F, and S6G), as previously reported in mutants that disrupt synaptic vesicle endocytosis (Bellen et al., 2010; Harris and Littleton, 2015; Koh et al., 2007; Zhang et al., 1998). Altogether, these data suggest that *cindr* may act at the nerve terminal to influence synapse maturation, expression of the vesicle-associated protein Synapsin, and regulation of synaptic vesicle dynamics.

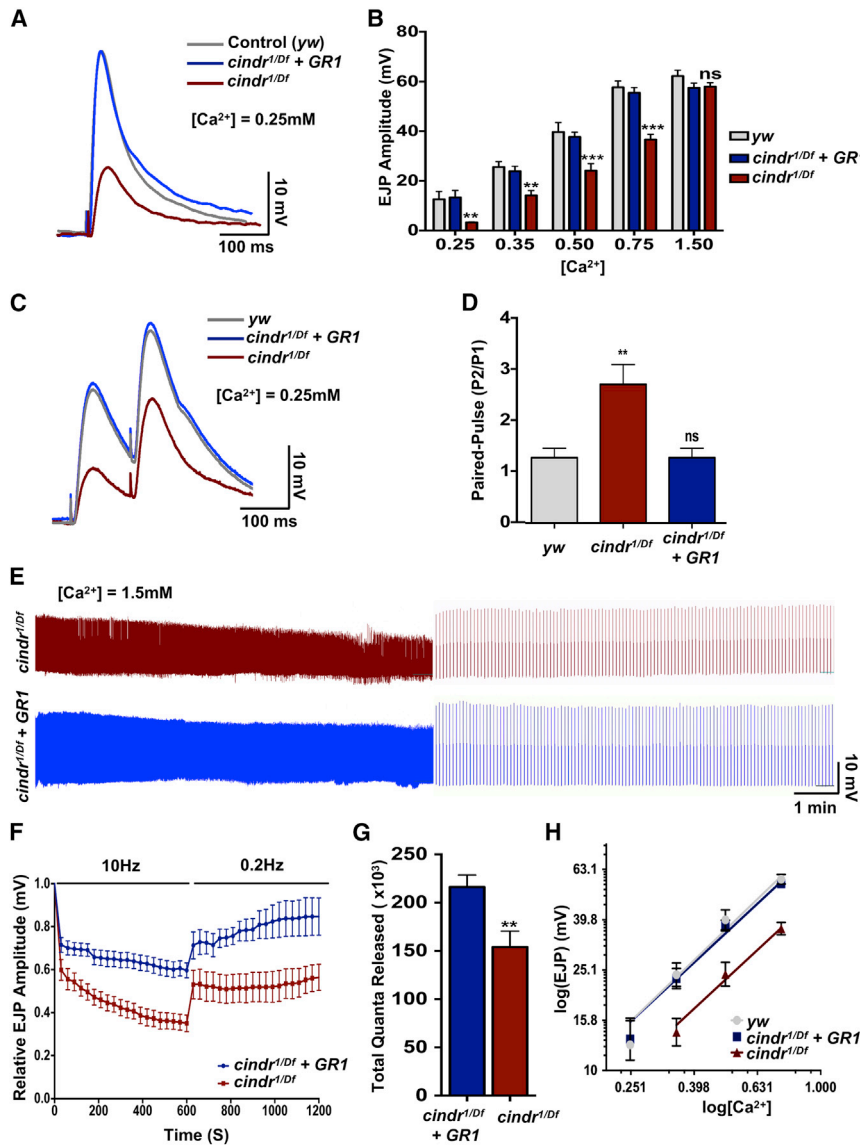


Figure 3. *cindr* Disrupts Neurotransmission and Synaptic Plasticity

(A) Based on neurophysiology studies at the larval neuromuscular junction, *cindr*^{1/DF} causes a reduction in excitatory junction potentials (EJPs). (B) EJP amplitude was quantified at different [Ca²⁺] and corrected for nonlinear summation. (C) *cindr*^{1/DF} enhances paired-pulse facilitation. (D) Quantification (n > 6) of paired-pulse facilitation. (E) *cindr*^{1/DF} accelerates synaptic depression during rapid stimulation (10 Hz) and attenuates recovery during a subsequent period of 0.2-Hz stimulation. Representative traces (1200 s) are shown. (F) Quantification of the rapid stimulation and recovery. Data were corrected for nonlinear summation and normalized to initial EJP amplitude. Two-way ANOVA was performed with Sidak's test, highlighting significant differences (p < 0.05) between genotypes after 150 s during 10-Hz stimulation and after 180 s during 0.2-Hz recovery. (G) Total estimated synaptic vesicle release during the 10-Hz stimulation experiment. Control or *cindr*^{1/DF} (n = 16) terminals released 220,000 ± 12,305 (mean ± SEM) versus 153,986 ± 16,469 vesicles, respectively. (H) Cooperativity plots reveal that *cindr* mutants require higher [Ca²⁺] to achieve the same EJP response, but the preserved slope (1.2) suggests intact calcium-vesicle release coupling. All error bars denote SEM. **p < 0.01; ***p < 0.001; ns, not significant. See also Figures S2 and S7.

***cindr* Is Required for Synaptic Transmission and Plasticity**

We next performed electrophysiological recordings to investigate whether *cindr* is required for normal synaptic function. We found that both amplitude and frequency of NMJ miniature excitatory junction potentials (mEJPs) in *cindr*^{1/DF} animals were similar to controls (Figures S7A–S7C). By contrast, in experiments performed using extracellular Ca²⁺ concentrations between 0.25 and 0.75 mM, the *cindr*^{1/DF} NMJ showed a reduction in evoked excitatory junction potential (EJP) amplitude (Figures 3A and 3B), and consistent results were seen in *cindr*¹ homozygotes (Figure S2E). However, when we increased extracellular calcium to 1.5 mM, the EJP amplitude was normalized. Although we accounted for potential nonlinear summation, our experimental design relying on current clamp cannot definitively exclude subtle differences in evoked release at higher Ca²⁺. *cindr* mutants

also showed defects in activity-dependent synaptic plasticity. To examine paired-pulse facilitation, we administered 2 current pulses separated by 50 ms. Facilitation was enhanced approximately 2-fold in either *cindr*^{1/DF} or *cindr*¹ animals (Figures 3C, 3D, and S2F). This result, in combination with the observed EJP reduction, suggests that loss of *cindr* compromises synaptic vesicle release probability. However, upon long-term (10 min), high-frequency (10 Hz) stimulation, *cindr*^{1/DF} animals exhibited a marked synaptic depression (Figures 3E and 3F), which is characteristic of mutants that are unable to sustain synaptic vesicle release because of defective endocytosis (Bellen et al., 2010; Harris and Littleton, 2015; Koh et al., 2007). Although we estimated a cumulative release of ~154,000 synaptic vesicles by the *cindr*^{1/DF} NMJ terminal during the 10-min trial, this was significantly less than controls (~220,000) (Figure 3G). Moreover, during a follow-up period of low-frequency stimulation (0.2 Hz), *cindr* mutants showed an initial recovery but subsequently plateaued (Figure 3F), suggesting that endocytic recycling persists but at a significantly diminished capacity. Overall, these neurophysiological data, along with the TEM results (described earlier) support a dual role for Cindr in both synaptic vesicle exocytosis and endocytosis at the larval NMJ.

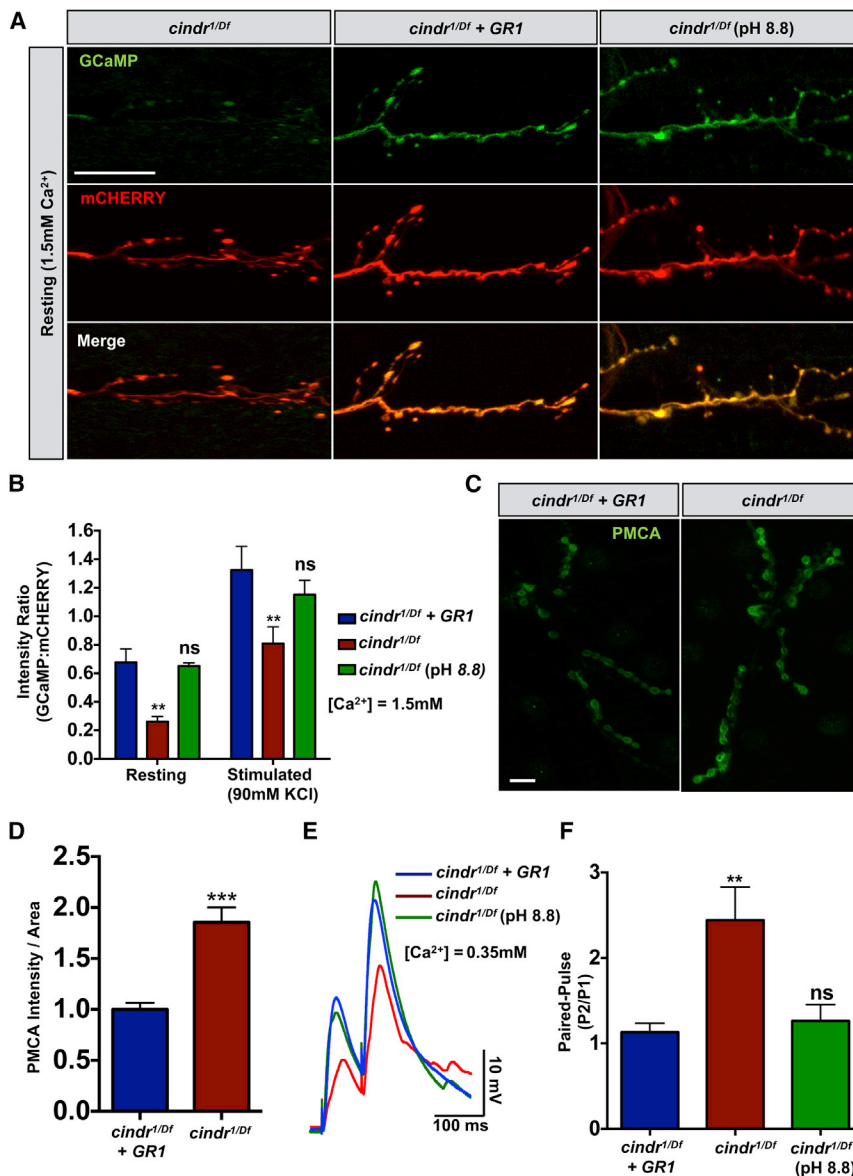


Figure 4. *cindr* Disrupts Calcium Homeostasis at the Synapse

(A and B) Calcium (Ca^{2+}) concentrations at the larval neuromuscular junction were assessed using the GCaMP sensor (green) compared with an mCherry internal standard (red). *cindr* mutants show reduced presynaptic Ca^{2+} under either resting or stimulated conditions. Increasing extracellular pH to 8.8 restores presynaptic Ca^{2+} .

(A) Representative GCaMP imaging from experiments at rest. Scale bar, 10 μm .

(B) Quantification of GCaMP experiments ($n > 9$ for all genotypes and conditions).

(C) Levels of PMCA protein (anti-PMCA) (green) at the larval neuromuscular junction are increased in *cindr^{1/DF}* mutants. Scale bar, 10 μm .

(D) Quantification ($n = 6$) of PMCA immunofluorescence.

(E) Increasing extracellular pH to 8.8 suppresses the *cindr^{1/DF}* paired-pulse facilitation phenotype.

(F) Quantification ($n = 6$) of paired-pulse experiment. All error bars denote SEM. ** $p < 0.01$; *** $p < 0.001$; ns, not significant. See also Figures S2 and S7.

experiments performed either at resting conditions or following stimulation with 90 mM potassium chloride, *cindr^{1/DF}* animals exhibit reduced cytoplasmic Ca^{2+} levels across a range of conditions (extracellular $[\text{Ca}^{2+}] = 0\text{--}1.5$ mM) (Figures 4A, 4B, S7D, and S7E).

As introduced earlier, we discovered and validated the PMCA as a Cindr binding partner (Table S1; Figure 1E), consistent with a potential role in calcium homeostasis. PMCA removes cytoplasmic Ca^{2+} , thereby maintaining appropriate concentrations for cell signaling and neurotransmission (Hajieva et al., 2018). Loss of *cindr* resulted in a 2-fold increase of PMCA expression at the NMJ (Figures 4C and 4D). We therefore hypothesized that

Endocytic mutants do not typically exhibit an acute exocytic defect. The exocytic phenotype observed in *cindr* mutants might therefore arise from either reduced cytosolic Ca^{2+} or dysfunction in the protein machinery required to couple Ca^{2+} to synaptic vesicle release (Frank et al., 2013; Harris and Littleton, 2015). To differentiate between these possibilities, we next examined the relationship between experimental extracellular Ca^{2+} concentrations ($[\text{Ca}^{2+}]$) and EJP. Although the Ca^{2+} cooperativity of release (slope) was not affected, the curve was shifted to the right in *cindr^{1/DF}* animals (Figure 3H). Thus, higher extracellular $[\text{Ca}^{2+}]$ is required to achieve the same evoked response, suggesting that loss of *cindr* leads to a reduced sensitivity to extracellular Ca^{2+} . We next evaluated presynaptic Ca^{2+} levels using a GCaMP sensor. The selected transgenic construct *UAS-GCaMP6m-P2A-mCherry* (Akerboom et al., 2012; Ugur et al., 2017) permits ratiometric normalization to an mCherry internal standard. In

increased PMCA activity might account for the reduced basal synaptic $[\text{Ca}^{2+}]$ in *cindr* mutants. PMCA exchanges extracellular H^+ for intracellular Ca^{2+} (Niggli et al., 1982; Smallwood et al., 1983); therefore, increasing extracellular pH would be expected to antagonize its function (Lnenicka et al., 2006). Basic conditions (pH 8.8) restored presynaptic Ca^{2+} at the *cindr^{1/DF}* NMJ (Figures 4A, 4B, and S7F), and both EJP and paired-pulse responses were normalized (Figures 4E, 4F, S7G, and S7H), consistent with a role for PMCA. Altogether, our results suggest that Cindr regulates neuronal Ca^{2+} homeostasis, potentially via PMCA, and that loss of *cindr* consequently impairs synaptic transmission and plasticity.

***cindr* Regulates Ubiquitin-Proteasome System Function**

Similar to our findings at larval NMJs, loss of *cindr* causes elevations of Synapsin and PMCA in the adult brain (Figures 5A, 5B,

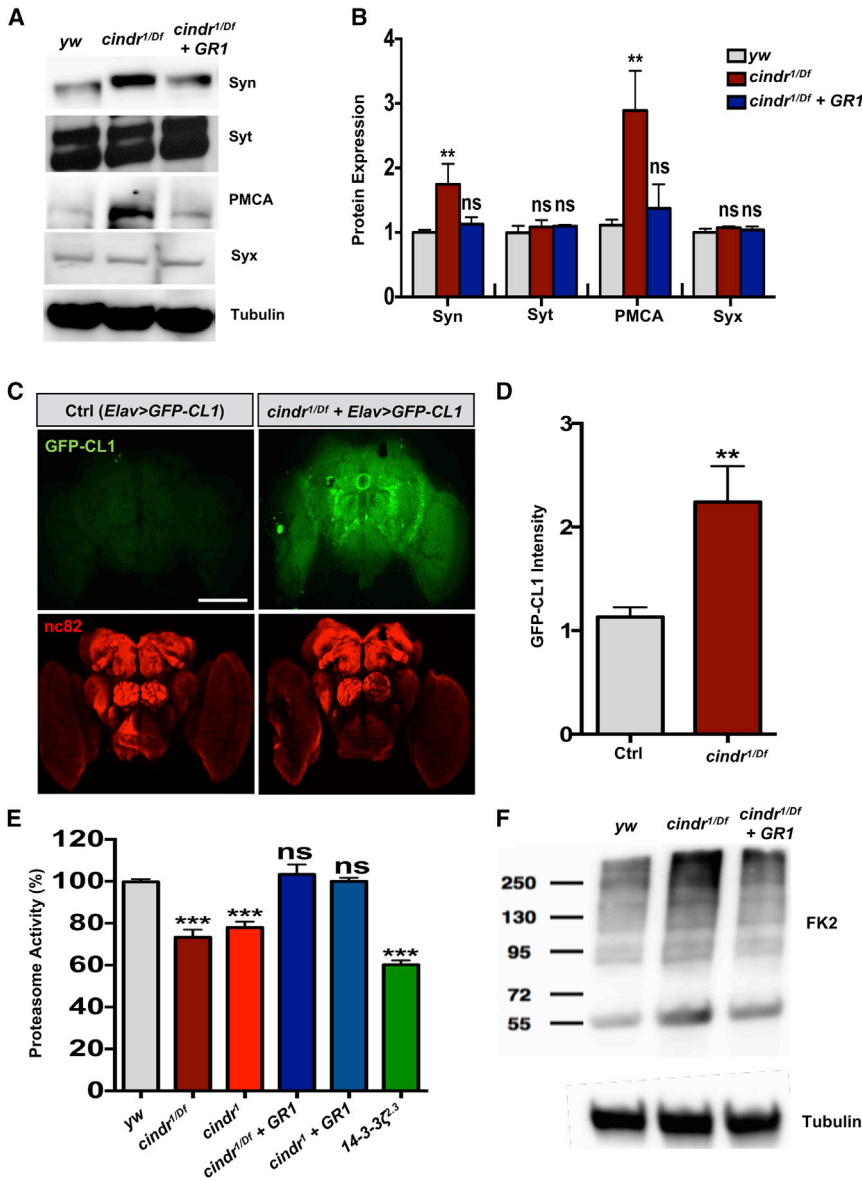


Figure 5. *cindr* Regulates Ubiquitin-Proteasome System Activity and Protein Turnover

(A) Synapsin (Syn) and PMCA protein levels are increased in *cindr*^{1/Df} adult heads. Other presynaptic proteins, including Synaptotagmin (Syt) and Syntaxin (Syx), were unchanged.

(B) Quantification of western blot results in (A) from at least 3 replicate experiments.

(C) In 5-day-old adults, the GFP-CL1 proteasome reporter is barely detectable (anti-GFP) (green) in brains from controls but is strongly increased in *cindr*^{1/Df}, indicating impaired ubiquitin-proteasome activity. Scale bar, 100 μ m.

(D) Quantification (n > 6) of GFP-CL1 intensity.

(E) Decreased proteasome activity is confirmed in both *cindr*^{1/Df} trans-heterozygous and *cindr*¹ homozygous animals, as well as 14-3-3^{2,3} homozygotes, using an *in vitro* assay that liberates a fluorescent peptide (Suc-LLVY-AMC) following cleavage. 3rd-instar larval homogenates were normalized for total protein levels and quantified (n > 6).

(F) *cindr* loss of function triggers an increase in polyubiquitinated proteins (FK2 antibody) in brains from 5-day-old adults. All error bars denote SEM. **p < 0.01; ***p < 0.0001; ns, not significant. See also Figure S8.

an *in vivo* reporter line in which GFP is fused with the CL1 degron, a signal sequence for ubiquitination and proteasome targeting (Pandey et al., 2007). When expressed in the adult brain using a pan-neuronal driver (*Elav>GFP-CL1*), the resulting GFP-CL1 fusion protein was barely detected, consistent with its rapid degradation (Figure 5C). By contrast, we observed a significantly increased signal of the *Elav>GFP-CL1* reporter in *cindr*^{1/Df} animals (Figures 5C and 5D), suggesting enhanced perdurance of the reporter because of impaired UPS-mediated turnover. Consistent results were also obtained using an *in vitro* proteasome activity assay in which a fluorescent peptide substrate (Suc-LLVY-AMC) is liberated following cleavage. Homogenates prepared from *cindr*^{1/Df} or *cindr*¹ larvae (normalized for total protein levels) showed a ~30% reduction in UPS activity (Figure 5E). Consistent with this, we detected a concomitant increase in polyubiquitinated proteins at the *cindr*^{1/Df} larval NMJ (Figures S8D and S8E) and in adult fly heads (Figure 5F), suggesting broader changes in the neuronal proteome. Overall, these data are consistent with a model in which loss of *cindr* disrupts UPS function and proteostasis, leading to elevations in PMCA and Synapsin and resulting impairments in Ca²⁺ homeostasis and synaptic function.

S2G, and S2H). Because *synapsin* and *PMCA* mRNA levels appear unaffected (Figure S8A), we hypothesized that Cindr may affect protein turnover of some binding partners via the ubiquitin-proteasome system (UPS). We found that Cindr associates with the 26S proteasomal subunit Rpt5 (Figure 1E), and CD2AP has been linked to proteasome function in other contexts (Kobayashi et al., 2004; Tsui and Pierchala, 2008). In addition, the UPS has previously been implicated to regulate both Synapsin levels (Fioravante et al., 2008; Lazarevic et al., 2011; Na et al., 2012) and synaptic function (Bingol and Sheng, 2011). Using a previously validated RNAi strain (L6w et al., 2013), we confirmed that knockdown of the essential proteasome subunit *RPT6A* (*Elav > RPT6^{RNAi}*) similarly resulted in elevated Synapsin and PMCA levels (Figures S8B and S8C). To determine whether proteasome activity is impaired in *cindr* mutants, we first employed

A large body of work links the UPS and altered neuronal proteostasis to AD pathogenesis (Yerbury et al., 2016). Specifically, prior studies of AD transgenic mouse models and human

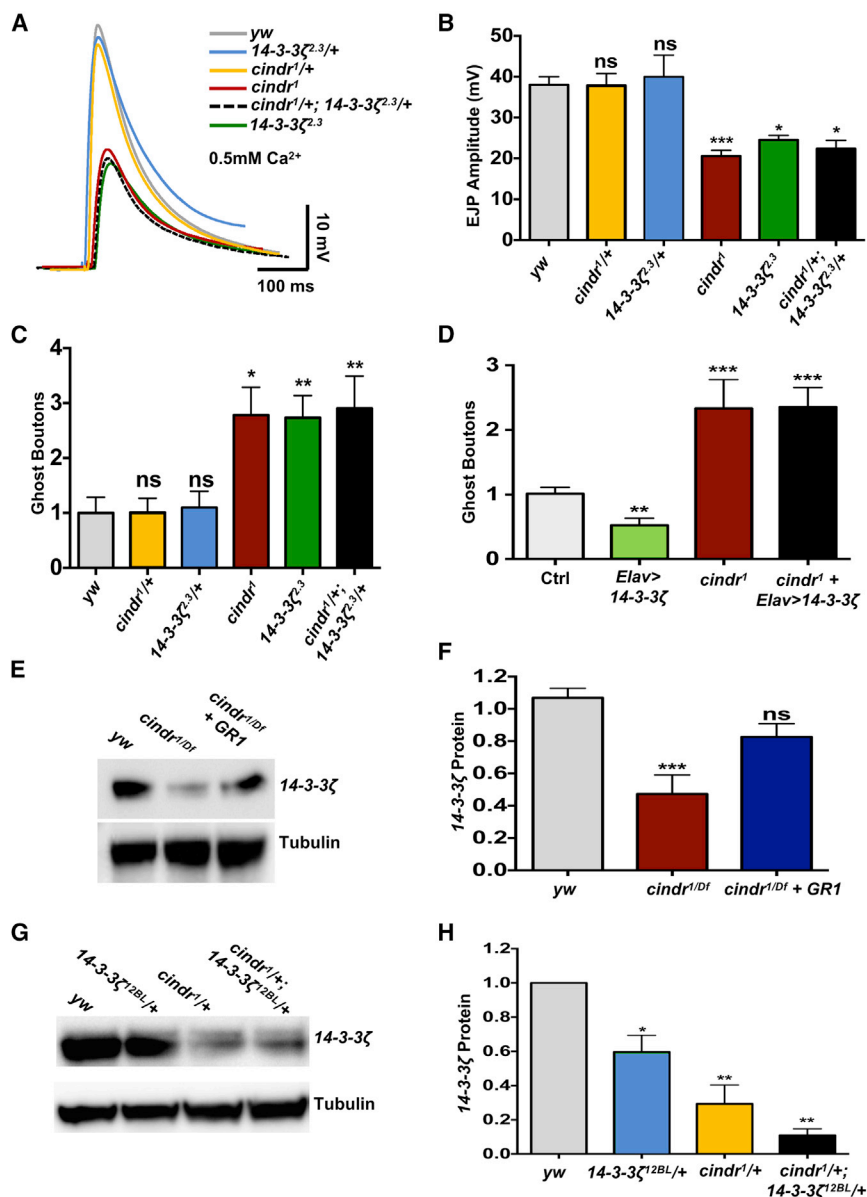


Figure 6. *cindr* Functions with 14-3-3 ζ to Affect Synapse Structure and Function

(A–D) 14-3-3 ζ loss of function phenocopies *cindr* at the larval neuromuscular junction, causing impaired synaptic transmission (A and B) and increased ghost bouton numbers (C). *cindr* and 14-3-3 ζ also show evidence of dominant genetic interactions (A–D), consistent with their coordinate function in a common pathway. Double-heterozygous allelic combinations of *cindr¹* with 14-3-3 $\zeta^{2,3}$ show EJP reductions (A and B) and increased NMJ ghost boutons (C) similar to *cindr^{1/Df}* or 14-3-3 $\zeta^{2,3}$ homozygotes.

(A and B) Representative traces (A) and quantification (B) ($n > 8$) of evoked excitatory junction potentials (EJPs).

(C) Quantification ($n > 6$) of ghost bouton numbers.

(D) Overexpression of 14-3-3 ζ reciprocally causes a reduction in ghost bouton numbers and *cindr* is epistatic. At least 6 animals were evaluated per genotype (*Elav-Gal4/Y* is present in all groups).

(E) *cindr* mutants cause a decrease in 14-3-3 ζ protein levels in the adult brain of 5-day-old animals.

(F) Quantification ($n > 5$) of 14-3-3 ζ protein expression.

(G) *cindr* shows a haploinsufficient requirement for 14-3-3 ζ protein expression in brains of 5-day-old animals, and *cindr/14-3-3 ζ* double heterozygotes show further reduction.

(H) Quantification ($n > 4$) of 14-3-3 ζ protein expression. All error bars denote SEM. * $p < 0.05$; ** $p < 0.01$; *** $p < 0.001$; ns, not significant. See also Figure S10.

function in *cindr* similarly converge to disrupt UPS activity in the *Drosophila* brain.

14-3-3 ζ Mediates *cindr* Function at the Synapse

To better understand the mechanism by which *cindr* regulates synaptic proteostasis and function, we examined another binding partner highlighted by IP-MS,

postmortem tissue indicate that Tau-paired helical filaments can disrupt proteasome function (Keck et al., 2003; Myeku et al., 2016). We previously found that RNAi-mediated knockdown of *cindr* enhances the neurotoxicity of human Tau in the fly retina (Shulman et al., 2014). Using the *cindr¹* null allele, we confirmed that *cindr* loss enhances age-dependent apoptotic neurodegeneration in the adult brain following pan-neuronal expression of human Tau (*Elav > Tau^{R406W}*) (Figures S9A and S9B). Because *cindr* mutants impair protein turnover via the UPS, we reasoned that this could explain the observed genetic interaction with Tau toxicity. To address this, we deployed the GFP-CL1 proteasome reporter in the Tau transgenic fly. Consistent with studies in mammalian AD models, Tau triggered a marked increase in detectable GFP reporter levels from adult fly brains (Figures S9C–S9E). Thus, Tau-mediated toxicity and loss of

the *Drosophila* ortholog of 14-3-3 ζ . The 14-3-3 ζ mutants have been reported to cause reduced EJPs and increased presynaptic facilitation (Broadie et al., 1997), similar to what we observe in *cindr* mutants. Moreover, 14-3-3 proteins have previously been shown to interact with and modulate UPS activity (Gu et al., 2018; Qureshi et al., 2013). Using a viable hypomorphic allele, 14-3-3 $\zeta^{2,3}$, we confirmed reduced NMJ synaptic strength (Figures 6A and 6B) and discovered that 14-3-3 $\zeta^{2,3}$ phenocopies the *cindr* ghost bouton phenotype (Figures 6C and S10A). Pan-neuronal overexpression of 14-3-3 ζ (but not *cindr*) caused a decrease in the number of immature boutons at the NMJ (Figures 6D and S10C). Moreover, *cindr* and 14-3-3 ζ showed evidence of dominant genetic interactions for both the ghost bouton and the EJP phenotypes. Specifically, in double-heterozygous allelic combinations of *cindr¹* with either 14-3-3 $\zeta^{2,3}$ (Figures 6A–6C)

or a null allele, *14-3-3 ζ ^{12BL}* (Figure S10B), we discovered reduced EJP amplitudes and increased NMJ ghost boutons similar to either *cindr¹/Df(3R)Exel3217* or *14-3-3 ζ ^{2,3}* homozygotes. This genetic interaction also suggests that 14-3-3 ζ and Cindr proteins may associate in a complex and function coordinately to promote synaptic transmission, consistent with their colP (Figure 1E). In addition, when *14-3-3 ζ* was overexpressed in a *cindr* mutant genetic background (*Elav-Gal4/+; cindr¹/UAS-14-3-3 ζ -cDNA, Df(3R)Exel3217*), the *cindr* mutant phenotype was epistatic, resulting in increased numbers of ghost boutons (Figure 6D). Consistent with these observations, we discovered that 14-3-3 ζ protein levels were sharply reduced in *cindr¹* animals, even in *cindr^{1/+}* heterozygotes (Figures 6E–6H). Our results suggest that Cindr is required for proper 14-3-3 ζ protein levels and that these proteins function together at the synapse.

Lastly, we investigated whether 14-3-3 ζ and *cindr* act cooperatively in regulating UPS function. Using the *in vitro* fluorometric proteasome activity assay, we first confirmed that UPS activity was similarly impaired in *14-3-3 ζ ^{2,3}* mutants (Figure 5E). Next, we examined PMCA and Synapsin protein levels. As expected, based on the genetic interactions described earlier, we found that *14-3-3 ζ* loss of function caused an increase in Synapsin and PMCA protein expression, whereas overexpression caused a reciprocal decrease (Figures S10D and S10E). Altogether, our findings reveal a regulatory pathway in which Cindr functions to maintain 14-3-3 ζ expression, which in turn targets Synapsin and PMCA for UPS-mediated degradation, thereby promoting synapse maturation and function.

CD2AP Has a Conserved Role in Synaptic Proteostasis

Our studies uncover a role for *cindr* in synaptic proteostasis and vulnerability for Tau-mediated neurotoxicity and therefore inform how CD2AP might contribute to AD susceptibility. To determine whether the function of *cindr* in regulating UPS is conserved in mammals, we obtained available *Cd2ap* germline knockout mice (Shih et al., 1999). CD2AP is expressed in the mammalian brain (Harrison et al., 2016), and homozygous null animals are viable with late-onset renal insufficiency. Western blots performed on brain homogenates prepared from 5-month-old *Cd2ap* null animals revealed elevations in the synaptic proteins Synapsin-1 and Synaptophysin, as well as PMCA (Figures 7A and 7B). Reciprocally, as in *Drosophila*, we discovered that 14-3-3 ζ protein is reduced. Moreover, these changes were accompanied by an approximately 20% decrease in proteasome activity (Figure 7C). These data highlight a conserved role for CD2AP in regulating UPS function and synaptic proteostasis in the mammalian brain.

Finally, we leveraged available data from a large clinical-pathological human cohort study to evaluate the potential translational relevance of our findings. The Religious Orders Study and Rush Memory and Aging Project (ROSMAP) recruits older adults without known dementia for annual clinical evaluations followed by brain autopsy and comprehensive neuropathological evaluations at the time of death (Bennett et al., 2018) (Table S2). Using selective reaction monitoring-MS proteomics, we quantified levels of CD2AP and homologs of Synapsin in postmortem cortical tissue samples from 838 brains and examined their relationship. Our results showed a highly significant

anti-correlation between CD2AP and Synapsin-1 ($p < 0.0001$, Figure 7D), and other human Synapsin paralogs (Figure S11). This relationship was robust to adjustment for AD pathology, age of death, sex, and postmortem interval (Tables S3 and S4). In a stratified analysis, the association between CD2AP and Synapsin levels was enhanced in the presence of AD pathology ($P_{\text{interaction}} = 0.005$, Figure S11). These data support a conserved role for CD2AP in synaptic proteostasis in the human brain.

DISCUSSION

CD2AP is an AD susceptibility gene (Lambert et al., 2013), but to date, its function in the adult nervous system is poorly defined. Our cross-species experimental strategy implicates Cindr in synaptic biology and defines potential links to AD pathogenic mechanisms. First, we show that Cindr is present at the synapse and interacts with other presynaptic proteins. Second, *cindr* loss of function causes impairments in synapse maturation and synaptic vesicle recycling and release. Third, the synaptic structural and functional defects are directly linked to requirements for Cindr in UPS-mediated protein turnover and Ca²⁺ homeostasis. Lastly, we show that Cindr functions with 14-3-3 ζ to regulate proteasome activity, and this role is likely conserved in mouse and human brains. Our results therefore enhance our understanding of *cindr/CD2AP* and suggest potential mechanisms for its contribution to AD susceptibility.

cindr Regulates Ca²⁺ Homeostasis, Neurotransmission, and Plasticity at Synapses

Synaptic loss is strongly associated with cognitive decline in AD (DeKosky and Scheff, 1990), and both A β and Tau have been linked to synaptic dysfunction (Spires-Jones and Hyman, 2014). In *Drosophila*, loss of *cindr* causes a combination of endocytic and exocytic synaptic defects. Prior studies have implicated *cindr/CD2AP* in endocytosis in other contexts (Cormont et al., 2003; Johnson et al., 2012; Lynch et al., 2003). Consistent with this, loss of *cindr* caused a reduced synaptic vesicle density at the NMJ and depression of synaptic responses during high-frequency stimulation, reminiscent of other genes implicated in endocytosis (Bellen et al., 2010; Harris and Littleton, 2015). Notable among these is *like-AP180* (Zhang et al., 1998), which is homologous to another AD susceptibility gene *PICALM*. Loss of *cindr* caused reduced evoked potentials and enhanced facilitation, which both result from diminished presynaptic Ca²⁺, possibly because of increased PMCA levels. Altered Ca²⁺ handling has also been linked to AD pathogenesis (Frere and Slutsky, 2018), in which PMCA has been implicated (Berrocal et al., 2012; Mata et al., 2011). PMCA is a Ca²⁺ efflux pump with an established requirement for neuronal Ca²⁺ homeostasis (Hajieva et al., 2018). We were able to rescue *cindr* phenotypes either directly through increasing extracellular [Ca²⁺] or indirectly by manipulating buffer pH to suppress PMCA activity; however, we cannot exclude the possibility that other Ca²⁺ channels or transporters may participate. Overall, we confirm a role for Cindr in synaptic vesicle endocytosis and recycling and highlight an unexpected requirement for presynaptic Ca²⁺ homeostasis and resulting vesicle exocytosis and release.

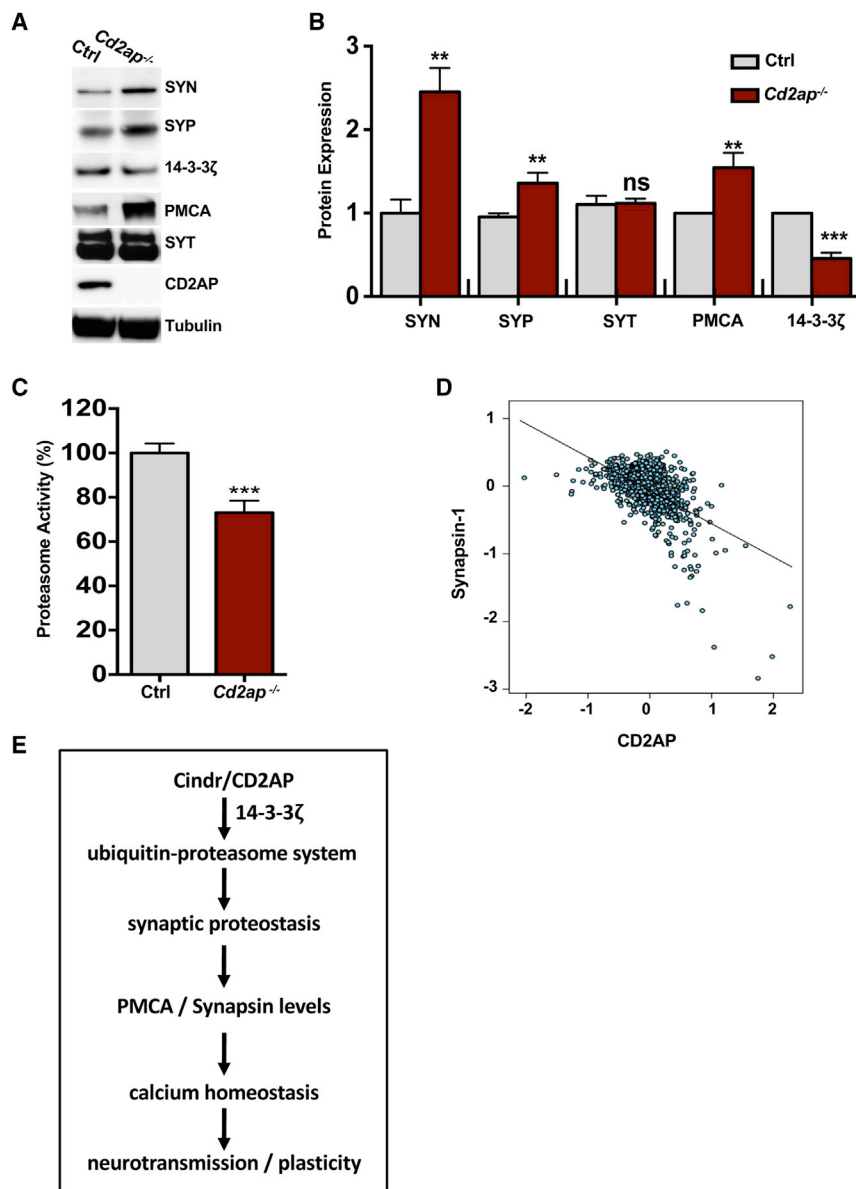


Figure 7. CD2AP Has a Conserved Role in Synaptic Proteostasis in Mammals

(A) Whole-brain homogenates from 5-month-old *Cd2ap*^{-/-} null mice show increased levels of Synapsin (SYN), Synaptophysin (SYP), and PMCA, but not Synaptotagmin (SYT), compared with wild-type control littermates. 14-3-3 ζ protein expression is reduced.

(B) Quantification of the western blot result (n > 3). All error bars denote SEM. **p < 0.01; ***p < 0.001; ns, not significant.

(C) *In vitro* proteasome assay reveals reduced ubiquitin-proteasome system activity in *Cd2ap*^{-/-} whole-brain homogenates normalized for total protein levels and quantified (n > 3).

(D) Cortical levels of CD2AP and Synapsin-1 proteins are significantly anti-correlated (r = -0.478, p < 0.0001), based on selective reaction monitoring-mass spectrometry proteomics from 838 human brain autopsies. The linear regression model relating CD2AP and Synapsin-1 was robust to adjustment for AD pathology, age of death, sex, and postmortem interval. See also Tables S2–S4 and Figure S11.

(E) Hypothetical model for proposed nervous system function of Cindr/CD2AP. CD2AP functions in concert with 14-3-3 ζ to target selected synaptic proteins for UPS-mediated degradation, promoting calcium homeostasis, synaptic neurotransmission, and plasticity.

Actin cytoskeletal dynamics have been implicated in synaptic vesicle recycling and plasticity, including at the *Drosophila* NMJ (Alicea et al., 2017; Piccioli and Littleton, 2014; Wang et al., 2010; Zhao et al., 2013b). Cindr is an actin binding protein, and we found that *cindr* loss of function stabilizes F-actin in the *Drosophila* nervous system, consistent with prior studies in both flies and human cells (Johnson et al., 2008; Welsch et al., 2005; Zhao et al., 2013a). Changes in actin could potentially influence many functions and phenotypes addressed in our study. Pharmacological manipulations that disrupt actin have been reported to attenuate ghost bouton formation (Piccioli and Littleton, 2014) and impair synaptic vesicle endocytosis (Kuromi and Kidokoro, 1998; Wang et al., 2010). Based on biochemical studies, actin may also bind and regulate human PMCA to modulate Ca²⁺ homeostasis (Dalghi et al., 2013). In mammals, Synapsins have

been shown to tether synaptic vesicles to the actin cytoskeleton, thereby regulating the vesicle reserve pool and activity-dependent, presynaptic plasticity (Cesca et al., 2010). In *Drosophila*, mutations in *synapsin* attenuate the formation of NMJ ghost boutons following stimulation (Vasin et al., 2014). While loss of *cindr* leads to an increase in Synapsin, this is unlikely to explain the accompanying ghost bouton formation, because Synapsin overexpression does not cause this phenotype. Although we identify elevations in Synapsin and other presynaptic proteins in *Cd2ap* null mice, it will be important in future work to directly confirm a conserved role for *Cd2ap* in the function of mammalian central synapses. In the rat peripheral nervous system, *Cd2ap* was implicated to participate in signal transduction during axonal outgrowth accompanying collateral sprouting, an important contributor to neuronal plasticity (Harrison et al., 2016).

CD2AP/cindr, 14-3-3 ζ , and Synaptic Proteostasis

The UPS plays an important role in normal synaptic function (Bingol and Sheng, 2011) and is strongly implicated in the altered proteostasis that accompanies neurodegenerative disorders, including AD (Yerbury et al., 2016). Proteasome activity is attenuated following loss of *cindr*, causing a concomitant increase in Synapsin and PMCA. While we document evidence of a more generalized increase in polyubiquitinated proteins, other

synaptic proteins (e.g., Synaptotagmin and Syntaxin) did not appear affected, consistent with at least some selectivity. Our observations in *Cd2ap* null mice support a conserved role in UPS regulation and synaptic protein turnover. Prior studies in both *Aplysia* (Fioravante et al., 2008) and rat brain (Lazarevic et al., 2011; Na et al., 2012) have implicated the UPS in the regulation of Synapsin levels. We confirmed that both PMCA and Synapsin are likely UPS targets in the *Drosophila* nervous system based on knockdown of a core proteasome subunit. In published work, application of proteasome inhibitors potentiated synaptic transmission at the larval NMJ (Speese et al., 2003). Our studies suggest that CD2AP/Cindr regulates the UPS in concert with 14-3-3 ζ . Loss of 14-3-3 ζ phenocopies *cindr*. Besides the previously reported attenuation of NMJ synaptic strength (Broadie et al., 1997), we show that 14-3-3 ζ mutants trigger ghost bouton formation and impair UPS activity, leading to elevations of Synapsin and PMCA. Moreover, Cindr associates and genetically interacts with 14-3-3 ζ , consistent with participation in a common regulatory pathway. 14-3-3 ζ protein abundance is exquisitely sensitive to changes in the *cindr* gene dosage. Prior investigations indicate that 14-3-3 ζ expression in the *Drosophila* nervous system likely depends on stabilization in protein complexes (Messaritou et al., 2010). CD2AP and its closely related mammalian paralog CIN85 have previously been linked to the UPS, particularly in the context of receptor tyrosine kinase signaling (Calco et al., 2014; Kobayashi et al., 2004; Soubeyran et al., 2002; Tsui and Pierchala, 2008). In addition, studies in both *Drosophila* cells and rat hippocampal culture demonstrate that 14-3-3 proteins possess chaperone-like activity and may promote degradation by delivering substrates to the proteasome (Qureshi et al., 2013; Sluchanko and Gusev, 2017; Yano et al., 2006). Conversely, in myeloma cell culture, 14-3-3 ζ antagonized proteasome assembly and activity (Gu et al., 2018), suggesting the possibility of a distinct, context-dependent impact on proteostasis. We therefore hypothesize that Cindr/CD2AP may serve as a scaffold to both stabilize 14-3-3 ζ and regulate its interactions with key synaptic targets (Figure 7E).

CD2AP and AD Susceptibility

GWASs have identified numerous susceptibility loci for AD (Lambert et al., 2013), but in most cases the responsible genes and relevant mechanisms remain obscure. In a *Drosophila* modifier screen targeting homologs of candidate genes at AD risk loci, we previously reported that *cindr* knockdown enhances Tau-induced neurodegeneration (Shulman et al., 2014). Our follow-up investigations in *Drosophila* link *cindr* to several inter-related neuronal mechanisms, including endocytosis, Ca²⁺ homeostasis, synaptic neurotransmission and plasticity, and the UPS, that are also strongly implicated in AD pathogenesis (Frere and Slutsky, 2018). Based on proteomics in a large human brain autopsy cohort, cortical CD2AP protein levels were anti-correlated with multiple Synapsins, and in the setting of AD neuropathology, this relationship was significantly enhanced. This result is consistent with a model in which UPS-dependent synaptic proteostasis is sensitive to CD2AP protein levels and AD pathological changes compromise proteasome activity. In AD post-mortem brain tissue, neurofibrillary tangles label strongly for both ubiquitin (Perry et al., 1987) and 14-3-3 ζ (Umahara et al.,

2004). Moreover, 14-3-3 ζ can bind misfolded and hyperphosphorylated Tau and modulate its aggregation (Qureshi et al., 2013; Sadik et al., 2009). Thus, our finding that *cindr* and 14-3-3 ζ cooperate in synaptic proteostasis in the *Drosophila* nervous system (Figure 7E) highlights an attractive hypothesis for their similar joint contribution to AD susceptibility.

Based on AD GWASs (Jansen et al., 2019; Kunkle et al., 2019; Lambert et al., 2013), the association signal at *CD2AP* is localized to several intergenic single-nucleotide polymorphisms, which are in strong linkage disequilibrium and positioned approximately 45 kb proximal to the gene promoter. In ROS-MAP, we previously found that the *CD2AP* risk allele is associated with neurofibrillary tangle pathological burden (Chibnik et al., 2018). Based on the largest available datasets (Battle et al., 2017; Ramasamy et al., 2014), *CD2AP* risk alleles are associated with moderately increased gene expression across various tissues, including in the brain. This may suggest that reduced *CD2AP* expression is protective for AD; however, this interpretation contradicts our experimental findings that *cindr/CD2AP* (1) is required for neuronal homeostasis and synaptic function and (2) knockdown enhances Tau-induced neurodegeneration. Moreover, the true causal variant or variants at the *CD2AP* locus remain unknown. A sequencing study identified several AD cases harboring a rare, *CD2AP* coding variant (K633R) predicted to be damaging (Vardarajan et al., 2015). Although this finding requires replication, it underscores the importance of fine mapping to definitively identify the responsible allelic variants and their mechanisms. Furthermore, because available brain RNA sequencing data are from bulk tissue, we are unable to differentiate the impact of *CD2AP* risk alleles on gene expression in neurons versus other cell types (e.g., astrocytes, endothelial cells, or microglia). *CD2AP* is broadly expressed, and although our studies define important neuronal requirements, prior work highlights complementary functions in other cell types and tissues (Bao et al., 2012; Cochran et al., 2015; Haglund et al., 2010). Finally, it is possible that susceptibility genes and the implicated biological pathways have dynamic and pleiotropic relationships with AD phenotypes, even flipping from protection to risk during distinct temporal or cell-type-specific disease phases (De Strooper and Karran, 2016). For example, while reduced neuronal [Ca²⁺] may attenuate synaptic strength and thereby increase vulnerability to early AD synaptic dysfunction, the identical perturbation may protect against late excitotoxic mechanisms (Palo et al., 2016; Spiess-Jones and Hyman, 2014). Thus, it is possible, if not likely, that *CD2AP* impinges on multiple targets and pathways to affect AD pathogenesis. In conclusion, although substantial challenges remain, functional dissection of susceptibility genes like *CD2AP* holds enormous promise for refinement of AD mechanistic models and development of improved therapeutics.

STAR★METHODS

Detailed methods are provided in the online version of this paper and include the following:

- KEY RESOURCES TABLE
- LEAD CONTACT AND MATERIALS AVAILABILITY

● **EXPERIMENTAL MODEL AND SUBJECT DETAILS**

- *Drosophila*
- Mouse
- Human Subjects

● **METHOD DETAILS**

- *Drosophila* stocks and husbandry
- Histology and immunofluorescence
- Western Blots
- TUNEL Assay
- Immunoprecipitation-Mass Spectrometry (IP-MS)
- GCaMP Ca²⁺ Imaging
- Electrophysiology
- Proteasome Activity Assay
- Transmission Electron Microscopy (TEM)
- Human brain proteomics

● **QUANTIFICATION AND STATISTICAL ANALYSIS**

● **DATA AND CODE AVAILABILITY**

SUPPLEMENTAL INFORMATION

Supplemental Information can be found online at <https://doi.org/10.1016/j.celrep.2019.07.041>.

ACKNOWLEDGMENTS

We thank R. Cagan, R. Johnson, U. Pandey, M. Feany, M. Bykhovskaia, R. Davis, and A. Shaw for providing antibodies and *Drosophila* stocks. The *CD2AP* null mouse was shared by A. Shaw. We thank Bloomington *Drosophila* Stock Center, the Vienna *Drosophila* RNAi Center, and FlyBase (Gramates et al., 2017). This study was supported by grants from the NIH (R01AG053960, R01AG050631, U01AG046161, U01AG061357, R01AG057339, R01AG033193, C06RR029965, P30AG10161, R01AG15819, R01AG17917, U01AG46152, R01AG36836, R01GM120033, R01AG36042, and RC236547); the Alzheimer's Association; the American Federation for Aging Research; the Huffington Foundation; and the Jan and Dan Duncan Neurological Research Institute at Texas Children's Hospital. The Pathology and Histology Core at Baylor College of Medicine is supported by NIH grant P30CA125123. The work was additionally supported by the Eunice Kennedy Shriver National Institute of Child Health & Human Development (U54HD083092). S.A.O. was supported by a Postdoctoral Enrichment Program Award from the Burroughs Wellcome Fund (BWF-1017399) and an Alzheimer's Association fellowship (AARFD-16-442630). J.M.S. was supported by a Career Award for Medical Scientists from the Burroughs Wellcome Fund. We thank Amit Chouhan, Hecmarie O. Melendez, and Yarong Li for technical assistance. The graphical abstract was created with the assistance of Biorender.com. We are grateful to Brandon Pekarek, Hui Zheng, and Khartik Venkatachalam for critical feedback and helpful discussions.

AUTHOR CONTRIBUTIONS

Conceptualization, S.A.O. and J.M.S.; Investigation, S.A.O., T.V.L., N.G., B.U., Z.Z., L.D., and Y.L.; Formal Analysis, L.Y.; Writing – Original Draft, S.A.O. and J.M.S.; Writing – Review & Editing, S.A.O., J.M.S., T.V.L., N.G., L.Y., B.U., V.P., P.L.D.J., D.A.B., H.J.B., and B.R.A.; Funding Acquisition, J.M.S., P.L.D.J., D.A.B., B.R.A., and H.J.B.; Resources, V.P., P.L.D.J., D.A.B., and B.R.A.; Supervision, J.M.S. and H.J.B.

DECLARATION OF INTERESTS

The authors declare no competing interests.

Received: December 28, 2018

Revised: May 30, 2019

Accepted: July 15, 2019

Published: August 13, 2019

REFERENCES

- Akerboom, J., Chen, T.W., Wardill, T.J., Tian, L., Marvin, J.S., Mutlu, S., Calderón, N.C., Esposti, F., Borghuis, B.G., Sun, X.R., et al. (2012). Optimization of a GCaMP calcium indicator for neural activity imaging. *J. Neurosci.* *32*, 13819–13840.
- Alicea, D., Perez, M., Maldonado, C., Dominicci-Cotto, C., and Marie, B. (2017). Cortactin Is a Regulator of Activity-Dependent Synaptic Plasticity Controlled by Wingless. *J. Neurosci.* *37*, 2203–2215.
- Alzheimer's Association (2016). 2016 Alzheimer's disease facts and figures. *Alzheimers Dement.* *12*, 459–509.
- Ataman, B., Ashley, J., Gorczyca, M., Ramachandran, P., Fouquet, W., Sigrist, S.J., and Budnik, V. (2008). Rapid activity-dependent modifications in synaptic structure and function require bidirectional Wnt signaling. *Neuron* *57*, 705–718.
- Bao, M., Hanabuchi, S., Facchinetti, V., Du, Q., Bover, L., Plumas, J., Chaperot, L., Cao, W., Qin, J., Sun, S.C., and Liu, Y.J. (2012). CD2AP/SHIP1 complex positively regulates plasmacytoid dendritic cell receptor signaling by inhibiting the E3 ubiquitin ligase Cbl. *J. Immunol.* *189*, 786–792.
- Battle, A., Brown, C.D., Engelhardt, B.E., Montgomery, S.B., et al.; GTEC Consortium; Laboratory, Data Analysis & Coordinating Center (LDACC)—Analysis Working Group; Statistical Methods groups—Analysis Working Group; Enhancing GTEC (eGTEC) groups; NIH Common Fund; NIH/NCI; NIH/NHGRI; NIH/NIMH; NIH/NIDA; Biospecimen Collection Source Site—NDRI (2017). Genetic effects on gene expression across human tissues. *Nature* *550*, 204–213.
- Bellen, H.J., Tong, C., and Tsuda, H. (2010). 100 years of *Drosophila* research and its impact on vertebrate neuroscience: a history lesson for the future. *Nat. Rev. Neurosci.* *11*, 514–522.
- Bennett, D.A., Buchman, A.S., Boyle, P.A., Barnes, L.L., Wilson, R.S., and Schneider, J.A. (2018). Religious Orders Study and Rush Memory and Aging Project. *J. Alzheimers Dis.* *64*, S161–S189.
- Berrocal, M., Sepulveda, M.R., Vazquez-Hernandez, M., and Mata, A.M. (2012). Calmodulin antagonizes amyloid- β peptides-mediated inhibition of brain plasma membrane Ca(2+)-ATPase. *Biochim. Biophys. Acta* *1822*, 961–969.
- Bingol, B., and Sheng, M. (2011). Deconstruction for reconstruction: the role of proteolysis in neural plasticity and disease. *Neuron* *69*, 22–32.
- Broadie, K., Rushton, E., Skoulakis, E.M., and Davis, R.L. (1997). Leonardo, a *Drosophila* 14-3-3 protein involved in learning, regulates presynaptic function. *Neuron* *19*, 391–402.
- Buszczak, M., Paterno, S., Lighthouse, D., Bachman, J., Planck, J., Owen, S., Skora, A.D., Nystul, T.G., Ohlstein, B., Allen, A., et al. (2007). The carnegie protein trap library: a versatile tool for *Drosophila* developmental studies. *Genetics* *175*, 1505–1531.
- Calco, G.N., Stephens, O.R., Donahue, L.M., Tsui, C.C., and Pierchala, B.A. (2014). CD2-associated protein (CD2AP) enhances casitas B lineage lymphoma-3/c (Cbl-3/c)-mediated Ret isoform-specific ubiquitination and degradation via its amino-terminal Src homology 3 domains. *J. Biol. Chem.* *289*, 7307–7319.
- Cesca, F., Baldelli, P., Valtorta, F., and Benfenati, F. (2010). The synapsins: key actors of synapse function and plasticity. *Prog. Neurobiol.* *91*, 313–348.
- Chibnik, L.B., White, C.C., Mukherjee, S., Raj, T., Yu, L., Larson, E.B., Montine, T.J., Keene, C.D., Sonnen, J., Schneider, J.A., et al. (2018). Susceptibility to neurofibrillary tangles: role of the PTPRD locus and limited pleiotropy with other neuropathologies. *Mol. Psychiatry* *23*, 1521–1529.
- Chouhan, A.K., Guo, C., Hsieh, Y.C., Ye, H., Senturk, M., Zuo, Z., Li, Y., Chatterjee, S., Botas, J., Jackson, G.R., et al. (2016). Uncoupling neuronal death and dysfunction in *Drosophila* models of neurodegenerative disease. *Acta Neuropathol. Commun.* *4*, 62.
- Cochran, J.N., Rush, T., Buckingham, S.C., and Roberson, E.D. (2015). The Alzheimer's disease risk factor CD2AP maintains blood-brain barrier integrity. *Hum. Mol. Genet.* *24*, 6667–6674.
- Cook, R.K., Christensen, S.J., Deal, J.A., Coburn, R.A., Deal, M.E., Gresens, J.M., Kaufman, T.C., and Cook, K.R. (2012). The generation of chromosomal

- deletions to provide extensive coverage and subdivision of the *Drosophila melanogaster* genome. *Genome Biol.* **13**, R21.
- Cormont, M., Metón, I., Mari, M., Monzo, P., Keslair, F., Gaskin, C., McGraw, T.E., and Le Marchand-Brustel, Y. (2003). CD2AP/CMS regulates endosome morphology and traffic to the degradative pathway through its interaction with Rab4 and c-Cbl. *Traffic* **4**, 97–112.
- Dalghi, M.G., Fernández, M.M., Ferreira-Gomes, M., Mangialavori, I.C., Malchiodi, E.L., Strehler, E.E., and Rossi, J.P. (2013). Plasma membrane calcium ATPase activity is regulated by actin oligomers through direct interaction. *J. Biol. Chem.* **288**, 23380–23393.
- De Strooper, B., and Karran, E. (2016). The Cellular Phase of Alzheimer's Disease. *Cell* **164**, 603–615.
- DeKosky, S.T., and Scheff, S.W. (1990). Synapse loss in frontal cortex biopsies in Alzheimer's disease: correlation with cognitive severity. *Ann. Neurol.* **27**, 457–464.
- Dustin, M.L., Olszowy, M.W., Holdorf, A.D., Li, J., Bromley, S., Desai, N., Wiedler, P., Rosenberger, F., van der Merwe, P.A., Allen, P.M., and Shaw, A.S. (1998). A novel adaptor protein orchestrates receptor patterning and cytoskeletal polarity in T-cell contacts. *Cell* **94**, 667–677.
- Fioravante, D., Liu, R.Y., and Byrne, J.H. (2008). The ubiquitin-proteasome system is necessary for long-term synaptic depression in *Aplysia*. *J. Neurosci.* **28**, 10245–10256.
- Frank, C.A., Wang, X., Collins, C.A., Rodal, A.A., Yuan, Q., Verstreken, P., and Dickman, D.K. (2013). New approaches for studying synaptic development, function, and plasticity using *Drosophila* as a model system. *J. Neurosci.* **33**, 17560–17568.
- Frere, S., and Slutsky, I. (2018). Alzheimer's Disease: From Firing Instability to Homeostasis Network Collapse. *Neuron* **97**, 32–58.
- Fu, Y., Zhu, J.Y., Richman, A., Zhao, Z., Zhang, F., Ray, P.E., and Han, Z. (2017). A *Drosophila* model system to assess the function of human monogenic podocyte mutations that cause nephrotic syndrome. *Hum. Mol. Genet.* **26**, 768–780.
- Godenschwege, T.A., Reisch, D., Diegelmann, S., Eberle, K., Funk, N., Heisenberg, M., Hoppe, V., Hoppe, J., Klagges, B.R.E., Martin, J.-R., et al. (2004). Flies lacking all synapsins are unexpectedly healthy but are impaired in complex behaviour. *Eur. J. Neurosci.* **20**, 611–622.
- Gramates, L.S., Marygold, S.J., Santos, G.D., Urbano, J.M., Antonazzo, G., Matthews, B.B., Rey, A.J., Tabone, C.J., Crosby, M.A., Emmert, D.B., et al.; the FlyBase Consortium (2017). FlyBase at 25: looking to the future. *Nucleic Acids Res.* **45** (D1), D663–D671.
- Gu, Y., Xu, K., Torre, C., Samur, M., Barwick, B.G., Rupji, M., Arora, J., Neri, P., Kaufman, J., Nooka, A., et al. (2018). 14-3-3 ζ binds the proteasome, limits proteolytic function and enhances sensitivity to proteasome inhibitors. *Leukemia* **32**, 744–751.
- Haglund, K., Nezis, I.P., Lemus, D., Grabbe, C., Wesche, J., Liestøl, K., Dikic, I., Palmer, R., and Stenmark, H. (2010). Cindr interacts with anillin to control cytokinesis in *Drosophila melanogaster*. *Curr. Biol.* **20**, 944–950.
- Hajjeva, P., Baeken, M.W., and Moosmann, B. (2018). The role of Plasma Membrane Calcium ATPases (PMCA) in neurodegenerative disorders. *Neurosci. Lett.* **663**, 29–38.
- Harris, K.P., and Littleton, J.T. (2015). Transmission, Development, and Plasticity of Synapses. *Genetics* **201**, 345–375.
- Harrison, B.J., Venkat, G., Lamb, J.L., Hutson, T.H., Drury, C., Rau, K.K., Bunge, M.B., Mendell, L.M., Gage, F.H., Johnson, R.D., et al. (2016). The Adaptor Protein CD2AP Is a Coordinator of Neurotrophin Signaling-Mediated Axon Arbor Plasticity. *J. Neurosci.* **36**, 4259–4275.
- Hata, Y., Slaughter, C.A., and Südhof, T.C. (1993). Synaptic vesicle fusion complex contains unc-18 homologue bound to syntaxin. *Nature* **366**, 347–351.
- Jansen, I., Savage, J., Watanabe, K., Bryois, J., Williams, D., Steinberg, S., Sealock, J., Karlsson, I., Hagg, S., Athanasiu, L., et al. (2019). Genetic meta-analysis identifies 9 novel loci and functional pathways for Alzheimer's disease risk. *Nat. Genet.* **51**, 404–413.
- Johnson, R.I., Seppa, M.J., and Cagan, R.L. (2008). The *Drosophila* CD2AP/CIN85 orthologue Cindr regulates junctions and cytoskeleton dynamics during tissue patterning. *J. Cell Biol.* **180**, 1191–1204.
- Johnson, R.I., Sedgwick, A., D'Souza-Schorey, C., and Cagan, R.L. (2011). Role for a Cindr-Arf6 axis in patterning emerging epithelia. *Mol. Biol. Cell* **22**, 4513–4526.
- Johnson, R.I., Bao, S., and Cagan, R.L. (2012). Interactions between *Drosophila* IgCAM adhesion receptors and cindr, the Cd2ap/Cin85 ortholog. *Dev. Dyn.* **241**, 1933–1943.
- Keck, S., Nitsch, R., Grune, T., and Ullrich, O. (2003). Proteasome inhibition by paired helical filament-tau in brains of patients with Alzheimer's disease. *J. Neurochem.* **85**, 115–122.
- Kim, J.M., Wu, H., Green, G., Winkler, C.A., Kopp, J.B., Miner, J.H., Unanue, E.R., and Shaw, A.S. (2003). CD2-associated protein haploinsufficiency is linked to glomerular disease susceptibility. *Science* **300**, 1298–1300.
- Klagges, B.R., Heimbeck, G., Godenschwege, T.A., Hofbauer, A., Pflugfelder, G.O., Reifegerste, R., Reisch, D., Schaupp, M., Buchner, S., and Buchner, E. (1996). Invertebrate synapsins: a single gene codes for several isoforms in *Drosophila*. *J. Neurosci.* **16**, 3154–3165.
- Kobayashi, S., Sawano, A., Nojima, Y., Shibuya, M., and Maru, Y. (2004). The c-Cbl/CD2AP complex regulates VEGF-induced endocytosis and degradation of Flt-1 (VEGFR-1). *FASEB J.* **18**, 929–931.
- Koh, T.W., Korolchuk, V.I., Wairkar, Y.P., Jiao, W., Evergren, E., Pan, H., Zhou, Y., Venken, K.J., Shupliakov, O., Robinson, I.M., et al. (2007). Eps15 and Dap160 control synaptic vesicle membrane retrieval and synapse development. *J. Cell Biol.* **178**, 309–322.
- Kunkle, B.W., Grenier-Boley, B., Sims, R., Bis, J.C., Naj, A.C., Boland, A., Vronskaya, M., van der Lee, S.J., Amlie-Wolf, A., Bellenguez, C., et al. (2019). Genetic meta-analysis of diagnosed Alzheimer's disease identifies new risk loci and implicates A β , tau, immunity and lipid processing. *Nat. Genet.* **51**, 414–430.
- Kuromi, H., and Kidokoro, Y. (1998). Two distinct pools of synaptic vesicles in single presynaptic boutons in a temperature-sensitive *Drosophila* mutant, shibire. *Neuron* **20**, 917–925.
- Lambert, J.C., Ibrahim-Verbaas, C.A., Harold, D., Naj, A.C., Sims, R., Bellenguez, C., DeStafano, A.L., Bis, J.C., Beecham, G.W., Grenier-Boley, B., et al.; European Alzheimer's Disease Initiative (EADI); Genetic and Environmental Risk in Alzheimer's Disease; Alzheimer's Disease Genetic Consortium; Cohorts for Heart and Aging Research in Genomic Epidemiology (2013). Meta-analysis of 74,046 individuals identifies 11 new susceptibility loci for Alzheimer's disease. *Nat. Genet.* **45**, 1452–1458.
- Lazarevic, V., Schöne, C., Heine, M., Gundelfinger, E.D., and Fejtova, A. (2011). Extensive remodeling of the presynaptic cytomatrix upon homeostatic adaptation to network activity silencing. *J. Neurosci.* **31**, 10189–10200.
- Liao, F., Jiang, H., Srivatsan, S., Xiao, Q., Lefton, K.B., Yamada, K., Mahan, T.E., Lee, J.M., Shaw, A.S., and Holtzman, D.M. (2015). Effects of CD2-associated protein deficiency on amyloid- β in neuroblastoma cells and in an APP transgenic mouse model. *Mol. Neurodegener.* **10**, 12.
- Littleton, J.T., Bellen, H.J., and Perin, M.S. (1993a). Expression of synaptotagmin in *Drosophila* reveals transport and localization of synaptic vesicles to the synapse. *Development* **118**, 1077–1088.
- Littleton, J.T., Stern, M., Schulze, K., Perin, M., and Bellen, H.J. (1993b). Mutational analysis of *Drosophila* synaptotagmin demonstrates its essential role in Ca²⁺-activated neurotransmitter release. *Cell* **74**, 1125–1134.
- Lnenicka, G.A., Grizzaffi, J., Lee, B., and Rumpal, N. (2006). Ca²⁺ dynamics along identified synaptic terminals in *Drosophila* larvae. *J. Neurosci.* **26**, 12283–12293.
- Lów, P., Varga, Á., Piracs, K., Nagy, P., Sztármári, Z., Sass, M., and Juhász, G. (2013). Impaired proteasomal degradation enhances autophagy via hypoxia signaling in *Drosophila*. *BMC Cell Biol.* **14**, 29.
- Lynch, D.K., Winata, S.C., Lyons, R.J., Hughes, W.E., Lehrbach, G.M., Wasinger, V., Corthals, G., Cordwell, S., and Daly, R.J. (2003). A Cortactin-CD2-associated protein (CD2AP) complex provides a novel link between

- epidermal growth factor receptor endocytosis and the actin cytoskeleton. *J. Biol. Chem.* 278, 21805–21813.
- MacLean, B., Tomazela, D.M., Shulman, N., Chambers, M., Finney, G.L., Frewen, B., Kern, R., Tabb, D.L., Liebler, D.C., and MacCoss, M.J. (2010). Skyline: an open source document editor for creating and analyzing targeted proteomics experiments. *Bioinformatics* 26, 966–968.
- Martin, A.R. (1955). A further study of the statistical composition on the end-plate potential. *J. Physiol.* 130, 114–122.
- Mata, A.M., Berrocal, M., and Sepúlveda, M.R. (2011). Impairment of the activity of the plasma membrane Ca^{2+} -ATPase in Alzheimer's disease. *Biochem. Soc. Trans.* 39, 819–822.
- McKhann, G., Drachman, D., Folstein, M., Katzman, R., Price, D., and Stadlan, E.M. (1984). Clinical diagnosis of Alzheimer's disease: report of the NINCDS-ADRDA Work Group under the auspices of Department of Health and Human Services Task Force on Alzheimer's Disease. *Neurology* 34, 939–944.
- Messaritou, G., Grammenoudi, S., and Skoulakis, E.M. (2010). Dimerization is essential for 14-3-3zeta stability and function *in vivo*. *J. Biol. Chem.* 285, 1692–1700.
- Minegishi, Y., Shibagaki, Y., Mizutani, A., Fujita, K., Tezuka, T., Kinoshita, M., Kuroda, M., Hattori, S., and Gotoh, N. (2013). Adaptor protein complex of FRS2 β and CIN85/CD2AP provides a novel mechanism for ErbB2/HER2 protein downregulation. *Cancer Sci.* 104, 345–352.
- Myeku, N., Clelland, C.L., Emrani, S., Kukushkin, N.V., Yu, W.H., Goldberg, A.L., and Duff, K.E. (2016). Tau-driven 26S proteasome impairment and cognitive dysfunction can be prevented early in disease by activating cAMP-PKA signaling. *Nat. Med.* 22, 46–53.
- Na, C.H., Jones, D.R., Yang, Y., Wang, X., Xu, Y., and Peng, J. (2012). Synaptic protein ubiquitination in rat brain revealed by antibody-based ubiquitome analysis. *J. Proteome Res.* 11, 4722–4732.
- National Institute on Aging; Reagan Institute Working Group on Diagnostic Criteria for the Neuropathological Assessment of Alzheimer's Disease (1997). Consensus Recommendations for the Postmortem Diagnosis Of Alzheimer's Disease. *Neurobiol. Aging* 18, S1–S2.
- Neumüller, R.A., Wirtz-Peitz, F., Lee, S., Kwon, Y., Buckner, M., Hoskins, R.A., Venken, K.J., Bellen, H.J., Mohr, S.E., and Perrimon, N. (2012). Stringent analysis of gene function and protein-protein interactions using fluorescently tagged genes. *Genetics* 190, 931–940.
- Niggli, V., Sigel, E., and Carafoli, E. (1982). The purified Ca^{2+} pump of human erythrocyte membranes catalyzes an electroneutral Ca^{2+} -H⁺ exchange in reconstituted liposomal systems. *J. Biol. Chem.* 257, 2350–2356.
- Packard, M., Koo, E.S., Gorczyca, M., Sharpe, J., Cumberledge, S., and Budnik, V. (2002). The *Drosophila* Wnt, wingless, provides an essential signal for pre- and postsynaptic differentiation. *Cell* 111, 319–330.
- Pallo, S.P., DiMaio, J., Cook, A., Nilsson, B., and Johnson, G.V.W. (2016). Mechanisms of tau and A β -induced excitotoxicity. *Brain Res.* 1634, 119–131.
- Pandey, U.B., Nie, Z., Batlevi, Y., McCray, B.A., Ritson, G.P., Nedelsky, N.B., Schwartz, S.L., DiProspero, N.A., Knight, M.A., Schuldiner, O., et al. (2007). HDAC6 rescues neurodegeneration and provides an essential link between autophagy and the UPS. *Nature* 447, 859–863.
- Perry, G., Friedman, R., Shaw, G., and Chau, V. (1987). Ubiquitin is detected in neurofibrillary tangles and senile plaque neurites of Alzheimer disease brains. *Proc. Natl. Acad. Sci. USA* 84, 3033–3036.
- Piccoli, Z.D., and Littleton, J.T. (2014). Retrograde BMP signaling modulates rapid activity-dependent synaptic growth via presynaptic LIM kinase regulation of cofilin. *J. Neurosci.* 34, 4371–4381.
- Qureshi, H.Y., Han, D., MacDonald, R., and Paudel, H.K. (2013). Overexpression of 14-3-3zeta promotes tau phosphorylation at Ser262 and accelerates proteasomal degradation of synaptophysin in rat primary hippocampal neurons. *PLoS ONE* 8, e84615.
- Ramasamy, A., Trabzuni, D., Guelfi, S., Varghese, V., Smith, C., Walker, R., De, T., Coin, L., de Silva, R., Cookson, M.R., et al.; UK Brain Expression Consortium; North American Brain Expression Consortium (2014). Genetic variability in the regulation of gene expression in ten regions of the human brain. *Nat. Neurosci.* 17, 1418–1428.
- Ryder, E., Ashburner, M., Bautista-Llacer, R., Drummond, J., Webster, J., Johnson, G., Morley, T., Chan, Y.S., Blows, F., Coulson, D., et al. (2007). The DrosDel deletion collection: a *Drosophila* genomewide chromosomal deficiency resource. *Genetics* 177, 615–629.
- Sadik, G., Tanaka, T., Kato, K., Yanagi, K., Kudo, T., and Takeda, M. (2009). Differential interaction and aggregation of 3-repeat and 4-repeat tau isoforms with 14-3-3zeta protein. *Biochem. Biophys. Res. Commun.* 383, 37–41.
- Sandoval, H., Yao, C.K., Chen, K., Jaiswal, M., Donti, T., Lin, Y.Q., Bayat, V., Xiong, B., Zhang, K., David, G., et al. (2014). Mitochondrial fusion but not fission regulates larval growth and synaptic development through steroid hormone production. *eLife* 3, 03558.
- Scheltens, P., Blennow, K., Breteler, M.M., de Strooper, B., Frisoni, G.B., Salway, S., and Van der Flier, W.M. (2016). Alzheimer's disease. *Lancet* 388, 505–517.
- Shih, N.Y., Li, J., Karpitskii, V., Nguyen, A., Dustin, M.L., Kanagawa, O., Miner, J.H., and Shaw, A.S. (1999). Congenital nephrotic syndrome in mice lacking CD2-associated protein. *Science* 286, 312–315.
- Shulman, J.M., Imboywa, S., Giagtzoglou, N., Powers, M.P., Hu, Y., Devenport, D., Chipendo, P., Chibnik, L.B., Diamond, A., Perrimon, N., et al. (2014). Functional screening in *Drosophila* identifies Alzheimer's disease susceptibility genes and implicates Tau-mediated mechanisms. *Hum. Mol. Genet.* 23, 870–877.
- Skoulakis, E.M., and Davis, R.L. (1996). Olfactory learning deficits in mutants for leonardo, a *Drosophila* gene encoding a 14-3-3 protein. *Neuron* 17, 931–944.
- Sluchanko, N.N., and Gusev, N.B. (2017). Moonlighting chaperone-like activity of the universal regulatory 14-3-3 proteins. *FEBS J.* 284, 1279–1295.
- Smallwood, J.I., Waisman, D.M., Lafreniere, D., and Rasmussen, H. (1983). Evidence that the erythrocyte calcium pump catalyzes a Ca^{2+} :nH⁺ exchange. *J. Biol. Chem.* 258, 11092–11097.
- Soubeyran, P., Kowanez, K., Szymkiewicz, I., Langdon, W.Y., and Dikic, I. (2002). Cbl-CIN85-endophilin complex mediates ligand-induced downregulation of EGF receptors. *Nature* 416, 183–187.
- Speese, S.D., Trotta, N., Rodesch, C.K., Aravamudan, B., and Broadie, K. (2003). The ubiquitin proteasome system acutely regulates presynaptic protein turnover and synaptic efficacy. *Curr. Biol.* 13, 899–910.
- Spires-Jones, T.L., and Hyman, B.T. (2014). The intersection of amyloid beta and tau at synapses in Alzheimer's disease. *Neuron* 82, 756–771.
- Stewart, B.A., Atwood, H.L., Renger, J.J., Wang, J., and Wu, C.F. (1994). Improved stability of *Drosophila* larval neuromuscular preparations in haemolymph-like physiological solutions. *J. Comp. Physiol. A Neuroethol. Sens. Neural Behav. Physiol.* 175, 179–191.
- Tsui, C.C., and Pierchala, B.A. (2008). CD2AP and Cbl-3/Cbl-c constitute a critical checkpoint in the regulation of ret signal transduction. *J. Neurosci.* 28, 8789–8800.
- Ubelmann, F., Burrinha, T., Salavessa, L., Gomes, R., Ferreira, C., Moreno, N., and Guimas Almeida, C. (2017). Bin1 and CD2AP polarise the endocytic generation of beta-amyloid. *EMBO Rep.* 18, 102–122.
- Ugur, B., Bao, H., Stawarski, M., Duraine, L.R., Zuo, Z., Lin, Y.Q., Neely, G.G., Macleod, G.T., Chapman, E.R., and Bellen, H.J. (2017). The Krebs Cycle Enzyme Isocitrate Dehydrogenase 3A Couples Mitochondrial Metabolism to Synaptic Transmission. *Cell Rep.* 21, 3794–3806.
- Umahara, T., Uchihara, T., Tsuchiya, K., Nakamura, A., Iwamoto, T., Ikeda, K., and Takasaki, M. (2004). 14-3-3 proteins and zeta isoform containing neurofibrillary tangles in patients with Alzheimer's disease. *Acta Neuropathol.* 108, 279–286.
- Vardarajan, B.N., Ghani, M., Kahn, A., Sheikh, S., Sato, C., Barral, S., Lee, J.H., Cheng, R., Reitz, C., Lantigua, R., et al. (2015). Rare coding mutations identified by sequencing of Alzheimer disease genome-wide association studies loci. *Ann. Neurol.* 78, 487–498.

- Vasin, A., Zueva, L., Torrez, C., Volfson, D., Littleton, J.T., and Bykhovskaia, M. (2014). Synapsin regulates activity-dependent outgrowth of synaptic boutons at the *Drosophila* neuromuscular junction. *J. Neurosci.* *34*, 10554–10563.
- Venken, K.J., Carlson, J.W., Schulze, K.L., Pan, H., He, Y., Spokony, R., Wan, K.H., Koriabine, M., de Jong, P.J., White, K.P., et al. (2009). Versatile P[acman] BAC libraries for transgenesis studies in *Drosophila melanogaster*. *Nat. Methods* *6*, 431–434.
- Verstreken, P., Ohyama, T., and Bellen, H.J. (2008). FM 1-43 labeling of synaptic vesicle pools at the *Drosophila* neuromuscular junction. *Methods Mol. Biol.* *440*, 349–369.
- Wagh, D.A., Rasse, T.M., Asan, E., Hofbauer, A., Schwenkert, I., Dürbeck, H., Buchner, S., Dabauvalle, M.C., Schmidt, M., Qin, G., et al. (2006). Bruchpilot, a protein with homology to ELKS/CAST, is required for structural integrity and function of synaptic active zones in *Drosophila*. *Neuron* *49*, 833–844.
- Wang, D., Zhang, L., Zhao, G., Wahlström, G., Heino, T.I., Chen, J., and Zhang, Y.Q. (2010). *Drosophila* twinfilin is required for cell migration and synaptic endocytosis. *J. Cell Sci.* *123*, 1546–1556.
- Welsch, T., Endlich, N., Gökce, G., Doroshenko, E., Simpson, J.C., Kriz, W., Shaw, A.S., and Endlich, K. (2005). Association of CD2AP with dynamic actin on vesicles in podocytes. *Am. J. Physiol. Renal Physiol.* *289*, F1134–F1143.
- Wittmann, C.W., Wszolek, M.F., Shulman, J.M., Salvaterra, P.M., Lewis, J., Hutton, M., and Feany, M.B. (2001). Tauopathy in *Drosophila*: neurodegeneration without neurofibrillary tangles. *Science* *293*, 711–714.
- Wong, C.O., Chen, K., Lin, Y.Q., Chao, Y., Duraine, L., Lu, Z., Yoon, W.H., Sullivan, J.M., Broadhead, G.T., Sumner, C.J., et al. (2014). A TRPV channel in *Drosophila* motor neurons regulates presynaptic resting Ca²⁺ levels, synapse growth, and synaptic transmission. *Neuron* *84*, 764–777.
- Yano, M., Nakamuta, S., Wu, X., Okumura, Y., and Kido, H. (2006). A novel function of 14-3-3 protein: 14-3-3zeta is a heat-shock-related molecular chaperone that dissolves thermal-aggregated proteins. *Mol. Biol. Cell* *17*, 4769–4779.
- Yerbury, J.J., Ooi, L., Dillin, A., Saunders, D.N., Hatters, D.M., Beart, P.M., Cashman, N.R., Wilson, M.R., and Ecroyd, H. (2016). Walking the tightrope: proteostasis and neurodegenerative disease. *J. Neurochem.* *137*, 489–505.
- Yoon, W.H., Sandoval, H., Nagarkar-Jaiswal, S., Jaiswal, M., Yamamoto, S., Haelterman, N.A., Putluri, N., Putluri, V., Sreekumar, A., Tos, T., et al. (2017). Loss of Nardilysin, a Mitochondrial Co-chaperone for α -Ketoglutarate Dehydrogenase, Promotes mTORC1 Activation and Neurodegeneration. *Neuron* *93*, 115–131.
- Yu, L., Petyuk, V.A., Gaiteri, C., Mostafavi, S., Young-Pearse, T., Shah, R.C., Buchman, A.S., Schneider, J.A., Piehowski, P.D., Sontag, R.L., et al. (2018). Targeted brain proteomics uncover multiple pathways to Alzheimer's dementia. *Ann. Neurol.* *84*, 78–88.
- Zhang, B., Koh, Y.H., Beckstead, R.B., Budnik, V., Ganetzky, B., and Bellen, H.J. (1998). Synaptic vesicle size and number are regulated by a clathrin adaptor protein required for endocytosis. *Neuron* *21*, 1465–1475.
- Zhao, J., Bruck, S., Cemerski, S., Zhang, L., Butler, B., Dani, A., Cooper, J.A., and Shaw, A.S. (2013a). CD2AP links cortactin and capping protein at the cell periphery to facilitate formation of lamellipodia. *Mol. Cell. Biol.* *33*, 38–47.
- Zhao, L., Wang, D., Wang, Q., Rodal, A.A., and Zhang, Y.Q. (2013b). *Drosophila* cyfip regulates synaptic development and endocytosis by suppressing filamentous actin assembly. *PLoS Genet.* *9*, e1003450.

STAR★METHODS

KEY RESOURCES TABLE

REAGENT or RESOURCE	SOURCE	IDENTIFIER
Antibodies		
mouse anti-SNORF1 (Synapsin)	DSHB	RRID: AB_2313867
rat anti-Elav	DSHB	RRID: AB_528218
mouse anti-Dlg	DSHB	RRID: AB_528203
mouse anti-Bruchpilot	DSHB	RRID: AB_2314866
mouse anti-Chaoptin	DSHB	RRID: AB_528161
mouse anti-Repo	DSHB	RRID: AB_528448
guinea pig anti-EPS15	Koh et al., 2007	N/A
rabbit anti-GFP	Thermo Fisher	A-11122
mouse anti-GFP (B-2) FITC-conjugated	Santa Cruz	SC-9996
rabbit anti-Leonardo (<i>Drosophila</i> 14-3-3 ζ)	Broadie et al., 1997	N/A
rat anti-Syntaxin	Hata et al., 1993	N/A
guinea pig anti-Synaptophysin	Synaptic Systems	Cat#101 004
mouse anti-Actin Clone C4	Sigma Aldrich	MAB1501
mouse anti-PMCA (5F10)	Abcam	AB2825
mouse anti-26S Proteasome p50 (112)-RPT5	Santa Cruz	RRID: SC_65745
mouse anti-FK1	Enzo	BML-PW8805-0500
mouse anti-FK2	Enzo	BML-PW8810-0100
mouse anti-Tubulin Clone DM1A	Sigma Aldrich	T6199
rabbit anti-Syt2	Littleton et al., 1993a	N/A
rabbit anti-14-3-3 ζ (Human)	Abcam	RRID: AB_51129
Alexa 488-conjugated secondary antibodies	Jackson ImmunoResearch Labs	RRID: AB_2338059
Alexa Cy3-conjugated secondary antibodies	Jackson ImmunoResearch Labs	RRID: AB_2338013
DyLight 649 Anti-Horseradish Peroxidase	Jackson ImmunoResearch Labs	N/A
Cy3 AffiniPure Goat Anti-Horseradish Peroxidase	Jackson ImmunoResearch Labs	Lot#137589
Critical Commercial Assays		
20S Proteasome Activity Assay Kit	Millipore	Cat#APT280
FragEL DNA Fragmentation Detection Kit Fluorescent - TdT Enzyme	Millipore	Cat#QIA39
Deposited Data		
Proteomic Data (CD2AP & Synapsin1-3)	This study	https://doi.org/10.7303/syn2580853
Experimental Models: Organisms/Strains		
<i>w¹¹¹⁸; 14-3-3ζ^{12BL}/CyO</i>	Bloomington Drosophila Stock Center	BDSC_9572; Flybase ID: FBal0065577
<i>w¹¹¹⁸; 14-3-3ζ^{2,3}/CyO</i>	Bloomington Drosophila Stock Center	BDSC_9573; Flybase ID: FBal0059634
<i>M{UAS-14-3-3ζ.ORF}ZH-86Fb</i>	FlyORF	FlyORF_F001492; Flybase ID: FBst0500670
<i>Syn⁹⁷</i>	Godenschwege et al., 2004	Flybase ID: FBal0155774
<i>UAS-Synapsin-GFP</i>	Vasin et al., 2014	N/A
<i>CH321-90L16-VK37 (GR2)</i>	Genetivision, Inc.	N/A
<i>P{PTT-GA}cindr^{CA06686} (cindr^{GFP})</i>	Bloomington Drosophila Stock Center	BDSC_50802; Flybase ID: FBal0211634
<i>UAS-Tau^{R406W}</i>	Wittmann et al., 2001	N/A
<i>Rpt6-RNAi: P{KK108783}VIE-260B</i>	Vienna Drosophila RNAi Center	VDRC_v100620; Flybase ID: FBal0235814

(Continued on next page)

Continued

REAGENT or RESOURCE	SOURCE	IDENTIFIER
UAS- <i>cindr</i> -PC-GFP	Johnson et al., 2008	N/A
UAS-CL1-GFP	Pandey et al., 2007	N/A
PBac{WH} <i>cindr</i> [f01073]	Exelixis at Harvard Medical School	Exelixis_f01073; Flybase ID: FBti0049715
PBac{RB}CG1554	Exelixis at Harvard Medical School	Exelixis_e03116; Flybase ID: FBst1014789
<i>yw</i> ; FRT82B <i>cindr</i> ¹ /TM6B	This study	N/A
CH321-75E06-VK37 (GR1)	This study	N/A
UAS-GCaMP6m-P2A-mCHERRY	Ugur et al., 2017	N/A
<i>w</i> ¹¹¹⁸ , Df(3R)Exel6217, P{XP-U} Exel6217/TM6B, Tb ¹	Bloomington Drosophila Stock Center	BDSC_7695; Flybase ID: FBst0007695
Cd2ap ^{KO} mouse	Shih et al., 1999	N/A
Recombinant DNA		
P[acman] BAC CH321-76E05 (<i>chr3R:30806623..30844282</i>)	Venken et al., 2009	N/A
P[acman] BAC CH321-90L16 (<i>chr3R:30787614..30871086</i>)	Venken et al., 2009	N/A

LEAD CONTACT AND MATERIALS AVAILABILITY

Further information and requests for resources and reagents should be directed to and will be fulfilled by the Lead Contact, Joshua M. Shulman (joshua.shulman@bcm.edu). All *Drosophila* strains generated for this study are available on request without restriction. No other unique reagents were generated in this study.

EXPERIMENTAL MODEL AND SUBJECT DETAILS**Drosophila**

Mixed sexes of flies (approximately 50% male and 50% female) were used for all experiments, where possible. Flies were raised on molasses-based food at 25°C with constant darkness unless otherwise noted. The full list of fly strains / genotypes used can be found in the [Key Resources Table](#). For clarity, detailed experimental genotypes are noted in Figure legends or with the relevant assay methods, below.

Mouse

All animals were treated in compliance with the US Department of Health and Human Services and Baylor College of Medicine IACUC guidelines. All experiments were performed in male mice of the same age, using animals maintained on a normal 12-hour light-dark cycle.

Human Subjects

The Religious Orders Study and Rush Memory and Aging Project (ROSMAP) participants were free of known dementia at enrollment, agreed to annual clinical evaluations, and signed an informed consent and Anatomic Gift Act donating their brains at death, approved by the Institutional Review Board at Rush University (Bennett et al., 2018). AD clinical diagnoses were made following National Institute of Neurological and Communicative Disorders and Stroke–Alzheimer’s Disease and Related Disorders Association recommendations (McKhann et al., 1984). AD neuropathologic diagnosis was made based on intermediate or high likelihood of AD by criteria from the National Institute on Aging and the Reagan Institute Working Group on Diagnostic Criteria for the Neuropathological Assessment of Alzheimer’s Disease (1997). Clinical and demographic features of the ROSMAP decedents included in this study can be found in [Table S2](#).

METHOD DETAILS**Drosophila stocks and husbandry**

All experimental genotypes are indicated in relevant figure legends or are specified with the description of the relevant assay methods, below. A complete list of fly strains used can be found in the [Key Resources Table](#). The *cindr*¹ null allele was generated by FLP-FRT recombination (Ryder et al., 2007; Cook et al., 2012) between two P-element strains, PBac{WH}*cindr*[f01073] and PBac{RB}CG1554, that flank the *cindr* locus (Figure 1A). The resulting *cindr*¹ null allele was recombined onto an FRT82B chromosome, and this strain was used for all experiments. Studies of *cindr* mutant flies used either *cindr*¹ homozygotes (*cindr*¹ / *cindr*¹)

or the transheterozygous genotype, *cindr¹ / Df(3R)Exel6217*, denoted in text and Figures as *cindr¹* or *cindr^{1/Df}*, respectively. A *yw*; *FRT82B* isogenic strain was used as the wild-type control strain since *cindr¹* was recombined into this genetic background. Transgenic rescue strains (*GR1* and *GR2*) were generated via ϕ C31-mediated integration of BAC constructs containing the entire *cindr* genomic locus. Transgenic flies were generated (38KBps, CH321-76E05, bacpac.Chori.org). Midi-Prep amplification of CH321-76E05 BAC was carried out overnight and plasmids were isolated and purified using the PureLink™ Hi-pure Plasmid DNA Purification Kit (Thermo Fisher Scientific). The purified *cindr* BAC was injected into VK37 fly embryos, allowing second chromosome specific integration of the *cindr* BAC to the second chromosome. 60 new founder/G0 males were crossed to virgin females and stocks were and balanced on CyO. Two transformants were obtained (Stock 17 and 21). A second BAC transgenic, CH321-90L16 BAC (90KBps), was generated by Genetivision, Inc. All studies using the transgenic *cindr* BAC, examined the genomic rescue construct in heterozygosity (e.g., *GR1 / +*; *cindr¹ / Df(3R)Exel6217* is abbreviated in Figures as *cindr^{1/Df} + GR1*). For survival assays, newly enclosed animals (20 flies per vial) and incubated at 25°C. Surviving animals were counted every 3 days. Each data point is a mean of 3 trials.

Histology and immunofluorescence

For hematoxylin and eosin staining, heads from adult flies were fixed in 8% glutaraldehyde (EM grade) and embedded in paraffin. 5 μ m frontal microtome sections were prepared (Leica) and treated as described in [Chouhan et al. \(2016\)](#). For immunostaining of the NMJ: Larvae were reared at 25°C and dissected at the third wandering instar stage. Larvae were dissected in Hemolymph-Like 3 (HL3) solution (110 mM NaCl, 5 mM KCl, 10 mM NaHCO₃, 10 mM MgCl₂, 5 mM trehalose, 30 mM sucrose, and 5 mM HEPES, pH 7.2) and fixed in 100% Methanol for 20 minutes. After fixation and washes in PBST (PBS containing 0.3% Triton X-100), larvae were blocked for 1 h in PBST containing 5% normal goat serum, incubated overnight with primary antibody at 4°C, washed, incubated with secondary antibodies for 2 h at room temperature, washed, and mounted in Vectashield (Vector Laboratories) for imaging. All NMJ studies were restricted to muscles 6/7 in abdominal section 2. Immunostaining of adult fly brains used a similar protocol except dissections were performed in 1x PBST and fixation was performed with 4% paraformaldehyde. For immunofluorescence, we used the following antibodies and dilutions (see also [Key Resources Table](#)): mouse anti-Dlg, 1:150; mouse anti-SNORF1 (Synapsin), 1:25; mouse anti-Bruchpilot (Brp), 1:100; mouse anti-Chaoptin; mouse anti-Repo, 1:500; Rat anti-Elav, 1:100; Guinea Pig anti-EPS15, 1:250; mouse anti-PMCA, 1:200; mouse anti-FK1, 1:100; Mouse anti-FK2, 1:500; rabbit anti-GFP, 1:250; mouse anti-GFP FITC conjugate, 1:100 (used for [Figures 1B, 1D, and S1D–S1F](#)); 1:250; DyLight 649 conjugated anti-horseradish peroxidase, 1:150; and CY3-conjugated anti-horseradish peroxidase, 1:100. Secondary antibodies used were all diluted at 1:500, including Alexa Fluor 488 goat anti-mouse, Alexa Fluor 488 goat anti-rabbit, and Alexa Fluor 546 goat anti-rabbit. Larva NMJ images were acquired using Z stack with a 0.67 step at 40x, 1.2 numerical aperture oil-immersion objective using a confocal microscope, while adult fly brain images were acquired using Z stack with a 2.00 step at 20x using a Confocal microscope. Immunostaining expression analysis at the NMJ were quantified by obtaining the average of 6 mean intensity per area of bouton per NMJ per genotype and normalizing to controls. For NMJ studies of Synapsin expression and ghost boutons, the following genotypes were used ([Figures 2C–2F](#)): (1, control) *yw*; (2) *cindr¹ / Df(3R)Exel6217*; or (3) *GR1 / +*; *cindr¹ / Df(3R)Exel6217*. For characterization of *14-3-3 ζ* loss-of-function and interaction with *cindr* genotypes were as follows ([Figure 6C](#)): (1) *yw*; (2) *cindr¹ / +*; (3) *14-3-3 ζ ^{2.3} / +*; (4) *cindr¹ / Df(3R)Exel6217*; (5) *14-3-3 ζ ^{2.3} / 14-3-3 ζ ^{2.3}*; (6) *14-3-3 ζ ^{2.3} / +*; *cindr¹ / +*. For complementary studies of *14-3-3 ζ* overexpression ([Figure 6D](#)), the experimental genotypes were as follows: (1) *Elav-Gal4 / Y*; +, (2) *Elav-Gal4 / Y*; *UAS-14-3-3 ζ* / +; (3) *Elav-Gal4 / Y*; *cindr¹ / Df(3R)Exel6217*; (4) *Elav-Gal4 / Y*; *cindr¹ / Df(3R)Exel6217*, *UAS-14-3-3 ζ* . GFP intensity of brain expressing GFP-CL1 were normalized to nc82 staining, and is reported relative to controls; the following genotypes were examined ([Figure 5A](#)): (1, control) *Elav-Gal4 / Y*; *UAS-GFP-CL1/+*; +) and (2, *cindr^{1/Df}*) *Elav-Gal4 / Y*; *UAS-GFP-CL1/+*; *cindr¹ / Df(3R)Exel6217*.

Western Blots

For western blots, we used the following additional antibodies and dilutions (see also [Key Resources Table](#)): anti-SNORF1 (Synapsin), 1:100; mouse anti-Actin, 1:500; rabbit anti-Syt2, 1:1000; rabbit anti-Leonardo (*Drosophila* 14-3-3 ζ), 1:1000; rabbit anti-GFP, 1:1000; rat anti-syntaxin, 1:1000, guinea-pig anti-synaptophysin, 1:500; rabbit anti-14-3-3 ζ (Human, used for [Figure 7A](#)), 1:1000; mouse anti-PMCA, 1:1000; mouse anti-PSD95, 1:500; mouse anti-tubulin clone DM1A, 1:1000; mouse anti-RPT5, 1:300; and mouse anti-FK2, 1:1000.

TUNEL Assay

TUNEL staining was performed using the FragEL DNA Fragmentation Detection Kit from Calbiochem (EMD Millipore Corp., MA USA). 10-day old adult fly brains were dissected in PBST and then fixed in 4% paraformaldehyde for 20 minutes on ice. Brains were washed with PBST 4 times for 15 minutes/wash and then blocked overnight at 4°C. Brains were then incubated in 100mM Sodium Citrate with 10% triton-x for 30 minutes at 65°C and then washed 3 times with PBST at room temperature. Brains were equilibrated (equilibration buffer) for 15 minutes at room temperature, and then incubated in a 1:9 mixture of Terminal deoxynucleotidyl transferase (Tdt) enzyme and Tdt Labeling Buffer for 2-3 hours at 37°C. Brains were washed 4 times for 15 minutes/wash at room temperature and then mounted on slide with Vectashield (with DAPI). Images were acquired using Z stack with a 2.00 step at 20x using a confocal microscope and apoptotic neurons were counted.

Immunoprecipitation-Mass Spectrometry (IP-MS)

cindr^{CA06686} fly heads were homogenized in lysis buffer (50 mM Tris pH7.4, 150 mM NaCl, 10% glycerol, 0.5% NP-40) containing complete protease inhibitor (Roche). Homogenized samples were subjected to centrifugation at 20,000 g for 20 min at 4°C. Supernatants were incubated in Chromotek-GFP-Trap Agarose Beads (Allele Biotechnology) in a rotator at 4°C. Cindr complex was eluted from the GFP-agarose beads and samples were subjected to nanoLC-MS/MS analysis with a nano-LC II (Thermo Scientific) coupled to Thermo Velos pro (Thermo Scientific) mass spectrometer as described in detail in Yoon et al. (2017). For confirmation of Cindr interactions, Cindr:GFP was immunoprecipitated with anti-GFP from head homogenates (*Elav-Gal4*; *UAS-cindr:GFP* / + and *Elav-Gal4* / *Y*; *UAS-cindr:GFP* / +). Control flies (Ctrl) were *Elav-Gal4* / + and *Elav-Gal4* / *Y*. 200 fly heads were grinded with a pestle in lysis buffer. After centrifugation at 15,000 g for 30 minutes to precipitate debris, brain lysate were collected and then incubated in Chromotek-GFP-Trap Agarose Beads (Allele Biotechnology) for 2-3 hours at 4°C. Beads were then centrifuged, washed with lysis buffer 6 times, and then 40ul of Lamelli buffer was added to samples for western blot. In Figure 1E, paired input (3%) and IP samples were run together for each of the two blots shown (Left & Right).

GCaMP Ca²⁺ Imaging

Protocol for Ca²⁺ imaging was modified from Wong et al. (2014). Third-instar larval fillets were prepared in ice-cold HL-3.1, which contained 110 mM NaCl, 5 mM KCl, 10 mM NaHCO₃, 10 mM MgCl₂, 5 mM trehalose, 30 mM sucrose, and 5 mM HEPES, pH 7.2. A total of 7 mM L-glutamic acid was added to HL-3.1 to desensitize glutamate receptors and prevent muscle contraction during the course of experiment. The VNCs was severed from the dorsal brain lobes to prevent peristalsis. Dissected fillets were allowed to equilibrate to room temperature in HL3.1 containing 1.5 mM Ca²⁺ for at least 15 min before imaging. Type 1b boutons on muscle 6 of abdominal segment A4 were brought to focus with a 25x water-immersion objective on an SP8 Leica Confocal microscope. Using Leica software, fluorescence signal was captured for mChERRY and for GCaMP6G (Average of 6 type 1B boutons/NMJ). The bath solution was then exchanged to HL3.1 containing 0.5mM CaCl₂. Two minutes after bath exchange, fluorescence signal was captured at the same settings. Bath solution was then further exchanged to nominally Ca²⁺ free HL3.1. Fluorescence signals were then captured again 2 min and 9 min after bath exchange. NMJ stimulation was carried out using 90mM K⁺ for 10 minutes as described by Verstreken et al. (2008). Recorded electrophysiology traces were analyzed using ImageJ software. Regions not containing an axon terminal and close to a region of interest (ROI) were selected as background. Mean pixel intensity from the background regions was subtracted from that of ROI for each fluorescence channel. Experiments were performed in *cindr*^{1/Df} (*Elav-Gal4* / + or *Y*; +; *cindr*¹ / *UAS-GCaMP6m-T2A-mCherry*, *Df(3R)Exel6217*) or *cindr*^{1/Df} + *GR1* controls (*Elav-Gal4* / + or *Y*; *cindr*¹ / *UAS-GCaMP6m-T2A-mCherry*, *Df(3R)Exel6217*).

Electrophysiology

ERG recordings were carried out as previously described (Sandoval et al., 2014). Briefly, adult flies were glued to a glass slide. A recording probe was placed on the surface of the eye, and a reference probe was inserted into the thorax. A fly eye was exposed to a flash of white light for 1 s. Responses were recorded and analyzed with AXONTM-pCLAMP8 software. For NMJ electrophysiology, free moving *Drosophila* larvae at the third-instar stage were dissected in HL3.1 buffer without Ca²⁺, and recordings were performed at various extracellular Ca²⁺ concentrations (Stewart et al., 1994). Ca²⁺ was provided as a chloride salt at the indicated concentrations. Larval motor axons were severed and Excitatory Junction Potentials (EJPs) were recorded from muscle 6 of abdominal segments A2 and A3 at room temperature. EJPs and mEJPs were analyzed using pClamp6 (Molecular Devices) and Mini Analysis Program (Synaptosoft) software, respectively. EJP amplitudes were corrected for nonlinear summation as previously described (Martin, 1955). For quantification of the resting membrane potential, we calculated the baseline from different recordings from different genotypes at various [Ca²⁺] concentrations. There were no differences in input resistance, time constant τ , and resting membrane potential among different genotypes tested in the experiments shown. Total quanta released during 10-Hz stimulation was determined by dividing the amplitude of the EJP by the average mini EJP amplitude. The neurophysiology studies of *cindr*^{1/Df} (Figures 3A–3G) use the following experimental genotypes: (1) *cindr*¹ / *Df(3R)Exel6217*; (2) Ctrl *yw*; or (3) *GR1* / +; *cindr*¹ / *Df(3R)Exel6217*. For the characterization of *14-3-3 ζ ^{2,3}* and interactions with *cindr* (Figures 6A and 6B), the following genotypes were used: (1) *yw*; (2) *cindr*¹ / +; (3) *14-3-3 ζ ^{2,3}* / +; (4) *cindr*¹ / *Df(3R)Exel6217*; (5) *14-3-3 ζ ^{2,3}* / *14-3-3 ζ ^{2,3}*; (6) *14-3-3 ζ ^{2,3}* / +; *cindr*¹ / +.

Proteasome Activity Assay

In vitro proteasome activity assays were carried out using the 20S proteasome activity Assay Kit protocol. 15 fillet preparations of 3rd instar larval were performed to remove fat bodies, lysed in lysis buffer and then centrifuged for 30 minutes at 15,000 rpm. The supernatant was obtained and concentration of protein per microliter was quantified using the Pierce BCA protein kit. Sample Lysates of equal protein amount were added to an assay mixture of proteasome substrate (Suc-LLVY-AMC), assay buffer and water (adding up to 100ul) and then incubated for 2 hours at 37°C in a 96 well plate. Fluorescence intensity was read using a 380/460 nm filter set in a fluorometer.

Transmission Electron Microscopy (TEM)

TEM of *Drosophila* adult retinæ and larval neuromuscular junctions were performed as in prior work (Ugur et al., 2017). *Drosophila* larval neuro muscular junctions (abdominal segment 3, muscle 6/7) were imaged following standard Electron Microscopy procedures

using a Ted Pella Bio Wave processing microwave with vacuum attachments. Briefly, whole 3rd instar larvae were dissected at room temperature in modified Karnovsky's fixative in 0.1 M Sodium Cacodylate buffer at pH 7.2 and subsequently fixed overnight to three days in the same fixative. The pre-fixed fillets were then irradiated in the fixed again, followed by 3 millipore water rinses, post-fixed with 1% aqueous Osmium Tetroxide, and rinsed again 3 times with millipore water. Concentrations from 30%–100% of Ethanol were used for the initial dehydration series, followed with Propylene Oxide as the final dehydrant. Samples were gradually infiltrated with 3 ratios of propylene oxide and Embed 812, finally going into 3 changes of pure resin under vacuum. Samples were allowed to infiltrate in pure resin overnight on a rotator. The samples were embedded into flat silicone molds and cured in the oven at 62°C for at least three days. The polymerized samples were thin-sectioned at 48–50 nm and stained with 1% uranyl acetate for ten minutes followed by 2.5% lead citrate for two minutes the day before TEM examination. For *Drosophila* retina ultrastructure was imaged using a Ted Pella Bio Wave processing microwave with vacuum attachments. Briefly, whole heads were dissected in accordance to preserve the brain tissue. The tissue was covered in 2% paraformaldehyde, 2.5% Glutaraldehyde, in 0.1 M Sodium Cacodylate buffer at pH 7.2. After dissection the heads were incubated overnight up to three days in the fixative on a rotator. The pre-fixed heads were then fixed again, followed by 3x millipore water rinses, post-fixed with 1% aqueous osmium tetroxide, and rinsed again 3x with millipore water. Concentrations from 25%–100% of Ethanol were used for the initial dehydration series, followed with Propylene Oxide as the final dehydrant. Samples were gradually infiltrated with 3 ratios of propylene oxide and Embed 812, finally going into 3 changes of pure resin under vacuum. Samples were allowed to infiltrate in pure resin overnight on a rotator. The samples were embedded into flat silicone molds and cured in the oven at 62°C for three days. The polymerized samples were thin-sectioned at 48–50 nm and stained with 1% uranyl acetate for ten minutes followed by 2.5% lead citrate for two minutes before TEM examination. Grids for both Retina and NMJ were viewed in a JEOL JEM 1010 transmission electron microscope at 80kV. Images were captured using an AMT XR-16 mid-mount 16 mega-pixel digital camera in Sigma mode. ImageJ was used to adjust contrast.

Human brain proteomics

Selective reaction monitoring-mass spectrometry proteomics was performed using frozen tissue from dorsolateral prefrontal cortex (DLPFC), as detailed in prior publications (Yu et al., 2018). Briefly, ~20 mg of brain tissue from each subject was homogenized in denaturation buffer (8M urea, 50 mM Tris-HCl pH 7.5, 10 mM DTT, 1 mM EDTA), and 400 µg aliquots were subjected to iodoacetamide alkylation and trypsin digestion, followed by solid phase extraction. At least 2 proteotypic peptides ¹³C/¹⁵N-labeled on carboxy-terminal lysine and arginine were selected to measure each target protein (New England Peptide, Gardner, MA). Following standard quality metrics, quantification was based on the peptide with the highest signal to noise ratio: CD2AP (VLFEYIPQNEDELELK), SYN1 (LGTEEFPLIDQTFYPNHK), SYN2 (SFRPDFVLIR), and SYN3 (SFKPDFILVR). Experiments were performed on a nano ACQUITY UPLC coupled to TSQ Vantage MS instrument, and data were analyzed using Skyline software (Skyline Software Systems, Inc., Herndon, VA) (MacLean et al., 2010). Peptide relative abundances were log₂-transformed and centered at the median.

QUANTIFICATION AND STATISTICAL ANALYSIS

Drosophila and mouse experimental data were analyzed using Prism, version 6.00 (Graph Pad Software, La Jolla, CA, USA). Statistical analyses relied on Student's t tests or Analysis of Variance (ANOVA), followed by Dunnett's post hoc test for multiple comparisons. The significance threshold was set at $p < 0.05$, and is noted in figures using the following convention: *, $p < 0.05$; **, $p < 0.01$; ***, $p < 0.001$. Otherwise, results are noted as "not significant" (ns). Error bars in all analyses represent the standard error of the mean (SEM). Sample sizes for all analyses are indicated in Figure legends, referring to the number of animals examined or replicate studies performed. Analyses of human proteomics data were performed using SAS version 9.4 (SAS Institute Inc, Cary, NC), and statistical significance was determined at α level of 0.05. Spearman correlations examined bivariate relationships between CD2AP and SYN1-3. Linear regression models examined the association of CD2AP with synaptic proteins after the adjustment for age, sex and postmortem intervals. In these models, the expression level of individual synaptic protein was the continuous outcome, and CD2AP expression was the predictor. The corresponding regression coefficient estimates the difference in synaptic protein level with every log₂ unit increase in CD2AP. We repeated the analyses by further adjusting for pathologic diagnosis of AD. Next, we augmented the models by adding an interaction term between pathologic AD diagnosis and CD2AP. A significant interaction term would suggest the CD2AP associations with synaptic proteins differ by AD diagnosis. Stratified linear regression analyses were also performed by AD diagnosis.

DATA AND CODE AVAILABILITY

Selective reaction monitoring-mass spectrometry proteomics and associated clinicopathologic data for ROSMAP human postmortem samples is available for request from the RADIC Research Resource Sharing Hub (<http://www.radc.rush.edu/>) and the AMP-AD Knowledge Portal on Synapse (<https://doi.org/10.7303/syn2580853>).